Femtosecond-to-nanosecond nonlinear spectroscopy of polymethine molecules

Richard S. Lepkowicz,* Claudiu M. Cirloganu, and Jie Fu

Center for Research and Education in Optics and Lasers and Florida Photonics Center of Excellence, College of Optics and Photonics, University of Central Florida, Florida 32816-2700

Olga V. Przhonska

Center for Research and Education in Optics and Lasers and Florida Photonics Center of Excellence, College of Optics and Photonics, University of Central Florida, Florida 32816-2700, and Institute of Physics, National Academy of Sciences, Prospect Nauki 46, Kiev, 03028, Ukraine

David J. Hagan and Eric W. Van Stryland

Center for Research and Education in Optics and Lasers and Florida Photonics Center of Excellence, College of Optics and Photonics, University of Central Florida, Florida 32816-2700, and Department of Physics, University of Central Florida, Orlando, Florida 32816-2700

Mikhail V. Bondar

Institute of Physics, National Academy of Sciences, Prospect Nauki 46, Kiev, 03028, Ukraine

Yuriy L. Slominsky and Alexei D. Kachkovski

Institute of Organic Chemistry, National Academy of Sciences, Murmanskaya 5, Kiev, 03094, Ukraine

Received May 16, 2005; accepted June 14, 2005

The linear and nonlinear optical properties of a series of polymethine molecules are investigated to study the effects of molecular structure and the host environment on overall nonlinear absorption performance. The linear characterization includes measuring the solvatochromic shifts between absorption and fluorescence peaks and studying the excited-state orientational diffusion kinetics. The nonlinear characterization involves measuring the excited-state absorption spectra with a femtosecond white-light-continuum pump–probe technique and performing Z scans and nonlinear transmission measurements from the picosecond to the nanosecond time regimes. The results of these experiments allow us to develop an energy-level structure for the polymethines, which accurately predicts nonlinear absorption properties from the picosecond to the nanosecond time regimes. From this model we are able to identify the key molecular parameters for improved nonlinear absorption.

OCIS codes: 190.4180, 140.3360, 190.4710.

1. INTRODUCTION

The development of new materials for nonlinear optical applications, such as optical switching, is an ongoing area of research.[1–3] Polymethine dyes (PDs) are promising compounds for applications requiring strong nonlinear absorption due to strong excited-state absorption (ESA) throughout the visible region. Our previous studies on the nonlinear absorption properties of PDs showed two key characteristics important for nonlinear transmission applications.[4,5] First, PDs have sufficiently large ground-state cross sections to completely populate the excited state (i.e., $\geqslant 10^{-18}$ cm^2 over the entire visible spectrum), and the cross section of the excited state is of the order of $\approx 10^{-15}$ cm^2 at the peak, which is comparable with the peak of the ground-state cross section. This produces some of the largest differences between excited-and ground-state cross sections ever measured (with ratios up to 200 at 532 nm).[5] Recently, a ratio of excited-to ground-state cross sections in a group of polymethines as large as 350 (at 470 nm) has been reported.[6] The second key characteristic is a saturation of the reverse saturable absorption (RSA) process, thus leading to saturable absorption at high fluences, which is detrimental for applications that depend on nonlinear absorption. Much of our efforts since our initial studies turned to developing a deeper understanding of the relationship between the molecular structure and the optical (both linear and nonlinear) properties[7–9] and excited-state dynamics.[10,11] From these studies, several new polymethine molecules were synthesized.

In the present study, we are concerned with measuring the linear and nonlinear optical properties of these new polymethines and studying the effects of molecular structure, such as conjugation length, bridge nature, and host

environment, on overall nonlinear absorption performance. All molecules were studied in up to eight different solvents (depending on solubility) to provide an adequate base to investigate solvent effects on ESA and excited-state dynamics.

A linear absorption analysis is performed for each molecule in all eight solvents. This analysis is discussed in Subsections 2.A and 2.B and includes determining the molar extinction coefficients at the peak of the linear spectra and solvatochromic shifts between absorption and fluorescence spectra. An accurate measurement of these material parameters is crucial for determining the nonlinear optical parameters. Making a meaningful comparison between the absorption properties of polymethine molecules of different conjugation lengths or bridge structures is not trivial. As can be seen from the linear absorption spectra shown in Fig. 1, a redshift of the linear absorption spectrum occurs as the conjugation length is increased, and the effects of different bridge structures also alters the spectrum. Thus, it is inadequate to study the nonlinear absorption properties of polymethines at a single wavelength to be able to make direct comparisons between molecules of different conjugation lengths. It is necessary to measure the ESA spectrum of each molecule and conduct the nonlinear absorption measurements at its peak spectral position. This was achieved by using a femtosecond white-light-continuum (WLC) transient absorption technique to measure the ESA spectrum of each molecule.[7] The experimental setup is discussed in Subsection 2.C, and the results are covered in Subsection 4.A.

The excited-state dynamics (lifetimes and orientational diffusion) are measured for each molecule in all host solvents. Although the orientational diffusion analysis does not affect the nonlinear absorption analysis directly, it does shed light on the geometry and flexibility of the molecule in the host environment. From these measurements we can see that the Stokes–Einstein–Debye (SED) model,[12] which treats the coupling between the solute and the solvent as hydrodynamic in nature, fails to adequately model the orientational diffusion of the polymethines. The modification to the SED model proposed by Perrin[13] is discussed along with dielectric friction[14] and possible hydrogen-bonding contributions.[15] From this analysis we can tell the type of boundary condition (e.g., slip or stick) the molecules have with the host environment. These issues are discussed in Subsection 4.B.

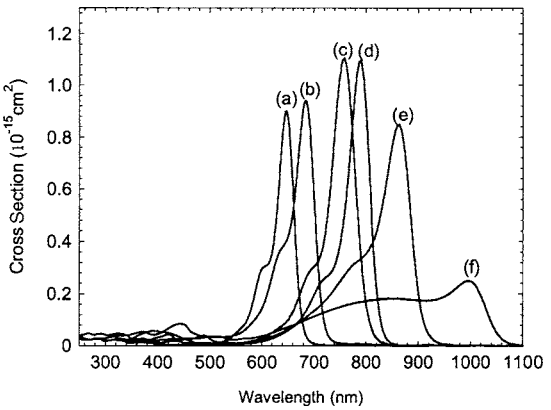

Fig. 1. Linear absorption spectrum in ethanol: (a) PD 2350, (b) PD 2410, (c) PD 3428, (d) PD 1952, (e) PD 824, and (f) PD 1659.

The nonlinear characterization focuses on using the insights gained from the linear characterization in conjunction with standard nonlinear optical measurement techniques such as picosecond and nanosecond Z scans,[16] along with picosecond and nanosecond nonlinear transmission experiments, to form a complete picture of the nonlinear absorption properties. The experimental setup for the nonlinear characterization is described in Subsection 2.D, and the results are covered in Subsections 3.A, 3.B, and 4.C.

The results of these experiments allow us to develop an energy-level structure for the polymethines, which accurately predicts nonlinear absorption properties from the picosecond to the nanosecond time regimes. From this model we are able to identify the key molecular parameters for improved nonlinear absorption. Furthermore, the study of each molecule at its ESA peak position allows for the development of a meaningful relationship between molecular structure (conjugation length of chromophore and bridge nature) and nonlinear absorption properties.

2. EXPERIMENT

A. Materials

The molecular structures of the PDs studied are shown in Fig. 2. Their chemical names and molecular structure information are given in Table 1. These PDs were synthesized at the Institute of Organic Chemistry, Kiev, Ukraine. Their molecular structures were confirmed by elemental analysis and nuclear magnetic-resonance spectra measurements. The synthesis of the unbridged PDs 2350 and 3428 is performed by standard methods as described in Ref. 17. Specific synthesis for the dyes with bridged polymethine chromophores (PDs 1952, 2410, 824, and 1659) is described in Ref. 18. The linear absorption spectra for all dyes in ethanol were recorded with a Varian Cary 500 spectrophotometer and are presented in Fig. 1.

The main spectroscopic properties of PDs are determined by the existence of a delocalized π-electron system in the polymethine chromophore (or polymethine chain) and symmetric terminal groups which themselves possess a delocalized π-electron system. The terminal groups for the polymethines are indolenine residues except for PD 1659, which has benzothiazolium terminal groups. The general distinction between the dyes can be made as a function of the polymethine chain length: di-carbocyanine (PD 2350), tricarbocyanines (PDs 1952, 2410, and 3428), tetracarbocyanine (PD 824), and pentacarbocyanine (PD 1659). An emphasis is placed on the tricarbocyanines, which differ by the bridge structure. PD 3428 has an unsubstituted (or unbridged) polymethine chromophore. PD 1952 has a five-membered cycle (or dimethylene bridge). Such cyclization leads to a decrease in the energy difference between the ground-state and the first excited-state levels [highest occupied molecular orbital (HOMO) and lowest unoccupied molecular orbital in the quantum-chemical analysis], resulting in a redshift of the absorption band.[8] PD 2410 has a five-membered vinylene cycle conjugated with the main π-electron system of the poly-

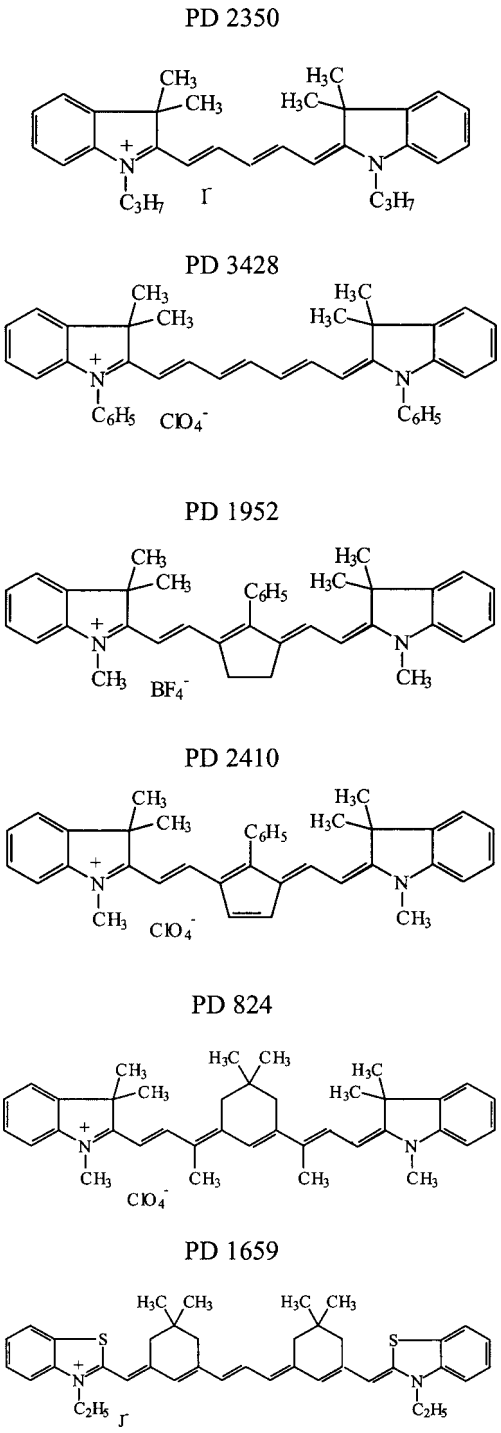

Fig. 2. Molecular structures.

methine chromophore. The vinylene bridge possesses its own π-electron system. The interaction between the orbitals of the bridge and the HOMO of the chain is substantial, which cause a decrease in the energy of the HOMO level and hence leads to a blueshift of the absorption band.[8] Complete quantum-chemical analysis for PDs 3428, 1952, and 2410, including charge and bond-length alternation in the ground and excited states, Franck–Condon relaxation, and results of anisotropy measurements, is presented in Ref. 8.

Pentacarbocyanine 1659 is characterized by an unusually broad absorption band as compared with the absorption of the dyes having a shorter polymethine chromophore; see Fig. 1. Detailed experimental and theoretical investigations of this molecule are performed in Ref. 9. We have shown that the absorption spectrum of PD 1659 in polar solvents, like ethanol, demonstrates a substantial band broadening represented by the growth of the short-wavelength shoulder. This is a strong indication of polar solvatochromism, which is typical for dyes with charge localization. We have come to the conclusion that an increase in the length of the polymethine chromophore leads to ground-state symmetry breaking and the appearance of the form with an asymmetrical distribution of the charge density.[9] Owing to the photochemical instability of PD1659, the only experimental measurements performed with this dye are picosecond Z scans and femtosecond WLC transient absorption.

B. Linear Absorption and Fluorescence Spectra Measurements

All molecules were studied in up to eight different host solvents (depending on solubility) to provide an adequate base to investigate specific and nonspecific solvent effects on ESA and excited-state dynamics. The eight solvents comprised four protic and four aprotic solvents. The four protic solvents are the saturated alcohols, R—OH: methanol (R=CH_3), ethanol (R=C_2H_5), butanol (R=C_4H_9), and pentanol (R=C_5H_{11}). The four aprotic solvents are N,N-dimethylformamide (DMF), N-methylformamide (MF), dimethyl sulfoxide (DMSO), and propylene carbonate (PC). The polarity of the solvents can be characterized by their orientational polarizability, Δf, which is given by $\Delta f=[\epsilon(0)-1]/[2\epsilon(0)+1]-(n^2-1)/(2n^2+1)$, where $\epsilon(0)$ is the static dielectric constant and n is the refractive index of the solvent.[19] The regular lengthening of the hydrocarbonic chain R in the protic solvents leads to an increase of solvent viscosity, dielectric relaxation time, and refractive index but a decrease of $\epsilon(0)$ and Δf. The key parameters for each solvent are given in Table 2.

The purpose of the linear absorption measurements is to accurately determine the ground-state cross section at the peak spectral position and at the wavelength where the nonlinear optical measurements are conducted (peak ESA) for each molecule in every solvent. Typically, nonlinear optical measurements (within the ESA band) are performed at wavelengths that are several hundred nanometers away from the linear peak position. Therefore, the ground-state cross section at this wavelength is 2 to 3 orders of magnitude smaller than at the peak. Owing to the limited dynamic range of the spectrophotometer, for accurate determination of the ground-state cross section at the ESA spectral peak, a series of measurements of concentrations from 10^{-7} to 10^{-5} M is performed. Information about the ground-state cross sections will be given in Subsections 4.A and 4.B along with the excited-state cross-section information.

Steady-state fluorescence spectra (using low concentrations, 10^{-6} M, to avoid reabsorption) were obtained with a Photon Technology International QuantaMaster spectrofluorimeter. The main goal of the fluorescence measure-

ments is to study the solvent-induced shifts of the spectral position of the peaks of both the absorption and the fluorescence spectra, which are known as solvatochromic shifts. Knowing how different solvents affect both the absorption and fluorescence spectra gives us insight into specific or nonspecific solvent effects, which are needed to make an accurate prediction of the orientational diffusion times. If only nonspecific interactions are affecting the molecule, the solvatochromic shifts should follow the Lippert–Mataga equation, which is given by

Table 1. Chemical Names and Molecular Structure Information

Chemical Name	Label	Volume (Å^3)[a]	Dimensions in x,y, and z Directions (Å)[b]	μ_{ge},S_0 to S_1 Transition Dipole Moment (Debye)[c]	μ_g,(S_0) and μ_e(S_1) Permanent Dipole Moments (Debye)[c]
2-[5-(1,3-dihydro-3,3-dimethyl-1-propyl-2H-indol-2-ylidene)-1,3-pentadienyl]-3,3-dimethyl-1-propylindolium iodide	PD 2350	470	18.6, 6, 4.5	14.3	0.3, 2.2
3,3,3,3-tetramethyl-1,1-diphenylindotricarbocyanine perchlorate	PD 3428	380	21, 6, 4.5	16.1	1.5, 3.5
1,3,3-trimethyl-2-(2-{2-phenyl-3[2-(1,3,3-trimethyl-1,3-dihydroindo-2-ylidene)ethylidene] cyclopent-1-enyl}vinyl)-3H-indolium tetrafluoroborate	PD 1952	420	23, 11, 6	15.9	1.2, 5.1
1,3,3-trimethyl-2-(2-{2-phenyl-3[2-(1,3,3-trimethyl-1,3-dihydroindo-2-ylidene)ethylidene] cyclopenta-1,4-dienyl}vinyl)-3H-indolium perchlorate	PD 2410	415	23, 12, 6	15.2	1.5, 4.5
2-[9-(1,3-dihydro-1,3,3-trimethyl-2H-indol-2-ylidene)-3,7-dimethyl-4,6-(2,2-dimethyltrimethylene)-1,3,5,7-nonatetraenyl]-1,3,3-trimethylindolium perchlorate	PD 824	615	23.5, 6.7, 7.5	17.6	0.8, 2.3
3,3-diethyl-9, 11,15,17-di (β,β-dimethyltrimethylene) thiapentacarbocyanine iodide	PD 1659	790	28.2, 10.4, 5.8	17.4[c]	0.7, 4.6[c]

[a]Molecular volumes were calculated as the minimal Van der Waals volumes by using the standard radii of the separate atoms or atomic groups (for example, CH_3,CH_2 residues), valence angles, and bond lengths.

[b]Axial dimensions are the distances along the x,y, and z coordinates between the most removed atoms. Calculations of the optimized molecular geometry have been performed in the AM1 approximation with the gradient 0.01 kcal/mol. It was found that the π-electron system of all molecules is practically planar in the X–Y plane, the bond lengths in the chain are almost equalized and equal $\approx$1.4 Å, and the calculated valence angles are $\approx$123°–125°. The methyl (CH_3) groups both in the indolenine residues and in the chain bridges (PD 824 and PD 1659) are out of the chromophore plane. The phenyl (C_6H_5) substituents near the nitrogen atoms (PD 3428) and in the mesoposition of the chain (PD 1952 and PD 2410) are placed perpendicularly to the plane of the main π-electron system. In contrast to rigidly fixed phenyl groups, the propylene (C_3H_7) substituents near the nitrogen atoms (PD 2350) are highly flexible for practically barrierless rotation around any carbon—carbon or nitrogen—carbon bonds.

[c]The ground, μ_g, and excited, μ_e, permanent dipole moments as well as transition moment, μ_{ge}, were calculated in the AM1 approximation. The excited-state function was built as the separation of the 25-lowest single excited configurations. The calculated magnitudes are given for the all-*trans* geometry. It is necessary to note that μ_{ge} is large and polarized along the polymethine chain, whereas μ_g and μ_e are relatively small and directed perpendicular to the chain. For PD 1659 the data are given for the form with the symmetrical charge distribution only.[9]

Table 2. Key Parameters for Protic and Aprotic Solvents

Solvent	Viscosity[a] (cp)	τ_D (ps)	n	$\epsilon(0)$	Δf
Protic R—OH					
Methanol R=CH_3	0.55	56	1.327	33.7	0.310
Ethanol R=C_2H_5	1.08	139	1.359	24.3	0.289
Butanol R=C_4H_9	2.59	482	1.397	17.4	0.263
Pentanol R=C_5H_{11}	3.51	727	1.407	14.8	0.252
Aprotic					
DMF	0.80	10	1.428	36.7	0.275
MF	1.65	170	1.430	182.4	0.289
DMSO	2.00	21	1.478	46.5	0.263
PC	2.53	43	1.420	65.0	0.287

[a]The viscosity, dielectric relaxation time τ_D, index of refraction n, and dielectric constant $\epsilon(0)$ values were taking from Ref. 14 and references therein.

$$\Delta\nu = \nu_a - \nu_f = \frac{2}{hc}(\Delta\mu_{eg})^2 a^{-3}\Delta f + \text{const.}, \quad (1)$$

where h is Planck's constant, c is the speed of light, a is the Onsager cavity radius in which the solute resides, $\Delta\mu_{eg}$ is the change in the permanent dipole moment from the ground to the excited states, Δf is the orientational polarizability of the solvent, and ν_a and ν_f are the peak spectral positions of the absorption and fluorescence spectra in wavenumbers (inverse centimeters), respectively.[19] If the shift ($\Delta\nu$) is a nonlinear function of polarity (Δf), then some type of specific solvent effect (e.g., hydrogen bonding) could be present. Since a broad range of solvents with different properties is being used, it is possible to narrow down the type of effect. The results of the fluorescence measurements will be discussed in context with the excited-state dynamics in Subsection 4.B.

C. Femtosecond and Picosecond Transient Absorption Spectroscopy

Femtosecond WLC transient absorption experiments to measure the ESA spectra were performed using the setup described in Ref. 7. The laser system used is a Clark-MXR 2001 Ti:sapphire amplified, frequency-doubled, erbium-doped fiber ring oscillator system pumping two optical parametric generator–amplifiers, OPG/As (Light Conversion Ltd., Model TOPAS), providing 100–120 fs (FWHM) pulses with independently tunable wavelengths of 0.55–2.2 μm. The pump beam was derived from the output of one OPG/A with pulse energies of the order of tens of microjoules and was tuned to near the peak of the linear absorption band for each dye. The probe beam was a subpicosecond WLC with an energy of 10s of nJ generated by our focusing a $\sim$2 μJ pulse from the other OPG/A at a wavelength of 1300 nm into a 2.5 mm thick calcium fluoride (CaF_2) plate.[20] The WLC was divided into a reference and a signal and monitored with a $\frac{1}{4}$ m spectrometer with a silicon dual photodiode array. To measure the shape of the ESA spectrum, we measured the WLC transmittance through the excited region of the sample with the WLC pulse delayed by $\approx$13 ps with respect to the pump pulse. This delay is considerably shorter than any excited-state population decay or reorientation times but should be much longer than the characteristic times for intraband relaxation in the excited state. The analysis of how to extract the absolute cross section and shape of the ESA spectrum from the continuum spectrum with and without the pump is given in Refs. 7 and 8.

The picosecond, two-color, polarization-resolved pump–probe setup has been described previously and is used to measure the excited-state dynamics of the polymethine molecules.[8] The laser system used for these experiments is a 10-Hz EKSPLA PL2143 Nd:YAG laser and an EKSPLA PG401/DFG optical parametric generator (OPG) tunable from 0.42 to 2.3 μm. The second harmonic of the Nd:YAG laser with a pulse width of 24 ps (FWHM) was used as the probe. The pump was the output of the OPG and was tuned near the peak of the linear absorption band for each dye. The energy range of the pump beam was between 2 and 20 μJ, whereas the probe was held to approximately 1 nJ. The probe beam was focused to a waist of 30 μm half-width $1/e^2$ maximum (HW1/e^2M), whereas the pump beam's focused waist was of the order of 150 μm HW1/e^2M. The pump beam was much larger than the probe beam to ensure that the probe beam senses a uniform excitation region in the sample. The pump irradiance was at least 40 times (in most cases several hundred times) larger than that of the probe beam. The probe beam could be temporally delayed with respect to the pump beam up to 15 ns, and its irradiance was kept low so as not to induce any nonlinearity in the sample. The pump and the probe beams were overlapped at a small angle ($\sim$5°) within the sample, so the probe beam could be separated after the sample from the pump. The pump polarization was adjusted with a half-wave plate and could be set to any angle with respect to the probe polarization. The probe beam was monitored before and after the sample by using large-area silicon photodiodes (1 cm diameter). In all cases, the samples were contained in 1 mm thick cuvettes, and the linear transmittance of the pump was >80%, to ensure uniform excitation through the length of the sample.

D. Single-Beam Nonlinear Transmission Measurements

The nonlinear transmission measurements include picosecond and nanosecond open-aperture Z-scan measurements[16] as well as measurements of transmittance versus input pulse energy. The Z scans were performed at low energies in order to study the RSA in the absence of saturation.[21] The picosecond and nanosecond Z scans were performed near the peak of the ESA spectrum. The samples had a linear transmission between 80% and 90% and were contained in 1 mm thick cells. The beam radius for the measurements is between 20 and 30 μm(HW $1/e^2$)], depending on wavelength, which means that all experiments are well within the thin-sample approximation.[16] The picosecond measurements spanned an energy range of 7 nJ (fluence: 1×10^{-3} J/cm^2; irradiance: 39 MW/cm^2) to 112 nJ (fluence: 14.7 $\times10^{-3}$ J/cm^2; irradiance: 127 MW/cm^2) and maximum change in transmission of 25%. The nanosecond measurements spanned an energy range of 26 nJ (fluence: 3 $\times10^{-3}$ J/cm^2; irradiance: 0.8 MW/cm^2) to 544 nJ (fluence: 46×10^{-3} J/cm^2; irradiance: 7.4 MW/cm^2).

The purpose of the nonlinear transmission measurements is to study the nonlinear absorption up to the saturation of the RSA process. The ability to gain information about the energy-level structure and dynamics from picosecond nonlinear transmission measurements has been previously demonstrated.[21–24] The picosecond measurements were performed with the second harmonic (532 nm) of the EKSPLA laser system discussed in Subsection 2.C. For the nanosecond nonlinear transmission measurements, we use two different pulse widths of 7 ns (FWHM) and 21 ns (FWHM) at 532 nm to gain information about the nonlinear absorption process near input levels where the RSA is reduced. The reasons for this will be discussed in Section 3. It is important to note that all the nonlinear transmission experiments reported here are performed at 532 nm (second harmonic of the Nd:YAG laser). Data taken at other wavelengths using either the picosecond OPG or the nanosecond optical parametric oscillator (OPO) proved to be extremely noisy at the high irradiance

levels compared with the 532 nm data, which is due to instabilities in the OPG and OPO systems.

The nanosecond measurements were performed with a Continuum Powerlite 9010, which is a single longitudinal mode, frequency-doubled, Nd:YAG laser, Q switched by a Pockels cell producing a 7 ns (FWHM) pulse width operating at a 10 Hz repetition rate. The repetition rate can be varied by altering the electrical signal to the Pockels cell. Also, by altering the Q-switch delay, one can increase the pulse width to 21 ns (FWHM). The OPO is a Continuum Sunlite EX, which is based on a beta-barium borate oscillator and amplifier pumped at 355 nm. This produces energies of several millijoules over the tuning range. The OPO beam is spatially filtered to obtain a Gaussian beam profile. The OPO signal beam is tunable from 450 to 710 nm and has a pulse width of 3–4 ns (FWHM). The idler beam is tunable from 710 to 1680 nm.

3. REVERSE SATURABLE ABSORPTION FROM PICOSECOND TO NANOSECOND

The ideology behind the modeling of RSA in polymethines is that the energy-level model will be simplest for short-pulse and low-energy experiments and will become more complex as the energy and pulse width are increased. For this reason the modeling starts with picosecond Z scans and expands to include nanosecond nonlinear transmission experiments. The population dynamics is described by multilevel rate equations.[1,23–26] For picosecond input pulses, a three-level system (singlet bands only) allows RSA to be modeled but often fails to match experimental data taken at high input fluences. The addition of a higher-lying fourth level allows for a better match for many materials.[21–24] The three- and four-level models are shown in Fig. 3, where the singlet energy levels are denoted by $S_{0,1,2,3}$. The ground-state cross section is given by σ_{01}, and the first and second excited-state cross sections are denoted by σ_{12} and σ_{23}, respectively. The excited-state lifetimes are given by τ_{ij} (meaning decay from level i to level j). A modification of this model that explains nanosecond data will be discussed in Subsection 3.B.

Note that it was found previously that the most intense ESA band in the visible region for PDs corresponds to the $S_1 \rightarrow S_5$ transition, whereas $S_1 \rightarrow S_2$ transitions are less

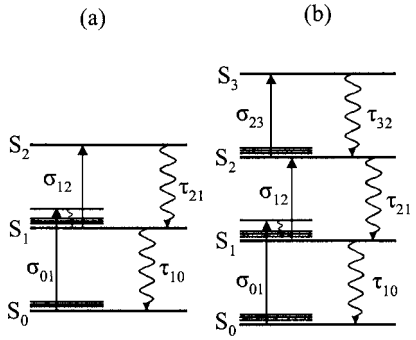

Fig. 3. (a) Three-level energy manifold schematic of an excited-state absorber; S_0 is the ground state, and S_1 and S_2 are the excited singlet states. (b) Schematic diagram of the four-level model of RSA.

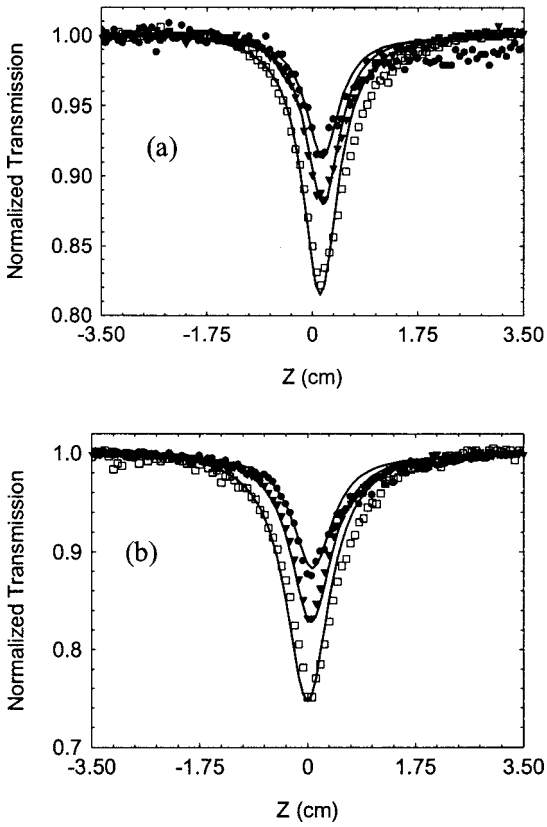

Fig. 4. Typical picosecond Z-scan results for (a) PD 824 in PC at fluences of 1.1×10^{-3} J/cm^2 (circles), 2.2×10^{-3} J/cm^2 (triangles), and 4.4×10^{-3} J/cm^2 (squares) and fitting parameters of $\sigma_{10}=7.8\times10^{-18}$ cm^2, $\sigma_{12}=3.0\times10^{-16}$ cm^2, and $\tau_{10}=0.4$ ns. (b) PD 1952 in ethanol at fluences of 2.9×10^{-3} J/cm^2 (circles), 5.7×10^{-3} J/cm^2 (triangles), and 9.8×10^{-3} J/cm^2 (squares) and fitting parameters of $\sigma_{10}=2.2\times10^{-18}$ cm^2, $\sigma_{12}=2.8\times10^{-16}$ cm^2, and $\tau_{10}=1.3$ ns.

intense and positioned in the infrared spectral range (1000–1400 nm).[7] At higher input fluences the second excited state can be populated, and the excited-state transition $S_2 \rightarrow S_n$ should be taken into account. Owing to fast (subpicosecond scale) internal conversion rates between high excited states, we can use the simplified labeling of transitions in our modeling (cross section σ_{12} and σ_{23} instead of σ_{15} and σ_{2n}), meaning that S_1 and S_2 are initial levels for ESA as the levels with the longest lifetimes (nanosecond and picosecond time scales). The final levels for ESA transitions in this paper are labeled as S_2 and S_3 for simplicity.

A. Picosecond Results and Modeling

The goal of the picosecond experiments is to determine the molecular parameters that affect nonlinear absorption and find their connections to the molecular structure and to the host solvent. The energy-level models developed from these experiments will be used as base models for the nanosecond experiments. In the nanosecond regime the models are inherently more complicated owing to slow processes, which require nanoseconds to form (for example, triplet-state populations and *cis–trans* conformational changes), whereas the picosecond measurements are insensitive to these longer processes. From the picosecond experiments we will determine the first and

higher-excited-state cross sections along with higher-excited-state dynamics of the five molecules under study.

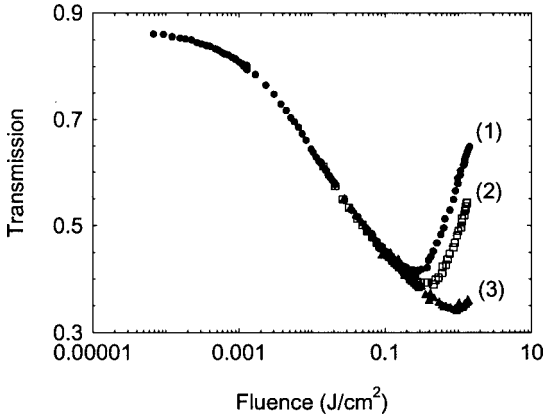

Fig. 5. Nonlinear transmission curve of PD 1952 in ethanol at different repetition rates: (1) 10 Hz, (2) 5 Hz, and (3) 1 Hz to demonstrate photodegradation effect.

In this subsection we will describe the experimental results and the fitting of the data using the models.

The first experiments carried out are low-energy Z scans, for which a simple, three-level (all singlets) energy structure may be used to model the results. This model is shown in Fig. 3(a). The Z scans are performed at the peak of the ESA spectrum and, from them, we determine the excited-state cross section (σ_{12}). Figure 4 shows the experimental results for the Z scans for two of the PDs with numerical fits using the three-level model.

The picosecond nonlinear transmission measurements are carried out to much higher fluences than the Z scans to determine higher-excited-state properties. To accurately model these results, it is necessary to add an additional, higher excited state. The corresponding four-level (all singlets) model is shown in Fig. 3(b). Primarily, we are concerned with determining the higher-excited-state cross section (σ_{23}) and lifetime (τ_{21}) from the fitting of this data.

When working with polymethine molecules, one must

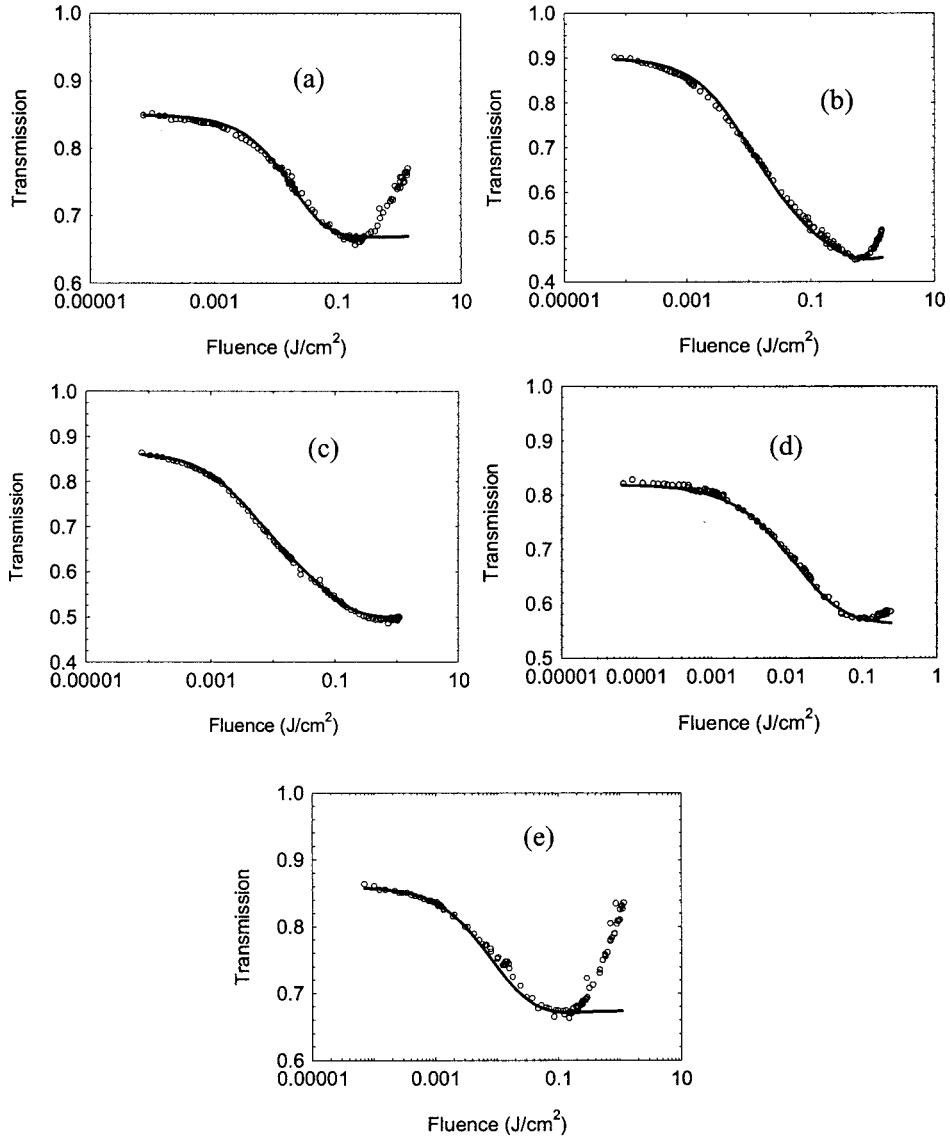

Fig. 6. Picosecond nonlinear transmission curves with fits using the four-level model shown in Fig. 3(b): (a) PD 2350 in pentanol, (b) PD 1952 in PC, (c) PD 3428 in DMF, (d) PD 2410 in ethanol, and (e) PD 824 in DMSO.

Table 3. Excited-State Dynamics

Dye	τ_{10} (ns)[a]	τ_r (ps)	τ_{21} (ps)	τ_{14} (ns)	τ_{gr} (ns)	τ_{40} (ns)
PD 2350						
Methanol	0.8	110	2	30	0.8	>100
Ethanol	1.0	230	1	30	1.1	>100
Butanol	1.4	440	4	11	1.7	>100
Pentanol	1.3	620	3	30	1.4	>100
DMF	1.5	310	11	7	1.9	>100
DMSO	1.6	310	11	9	1.9	>100
MF	1.1	400	9	7	1.3	>100
PC	1.3	480	2	25	1.3	>100
PD 1952						
Methanol	1.0	140	3	2.0	2.1	>100
Ethanol	1.3	310	3	1.2	10	>100
Butanol	1.2	590	4	DNF[b]	DNF	DNF
Pentanol	0.9	790	4	DNF	DNF	DNF
DMF	1.3	270	8	3.0	2.3	>100
DMSO	1.5	430	4	1.9	7.0	>100
MF	1.2	460	4	1.4	9.0	>100
PC	1.3	580	3	1.5	11.0	>100
PD 2410						
Methanol	1.2	160	3	NA[c]	NA	NA
Ethanol	1.4	370	7	NA	NA	NA
DMSO	1.3	360	7	61	1.4	>100
PC	0.7	620	3	13	0.8	>100
PD 3428						
Methanol	1.0	220	9	2	1.9	>100
Ethanol	1.3	350	17	1.9	4.0	>100
Butanol	1.3	610	17	2.8	2.5	>100
DMF	1.3	350	12	1.9	3.7	>100
DMSO	1.6	780	16	DNF	DNF	DNF
MF	1.2	500	15	1.8	3.9	>100
PC	1.60	630	15	2.6	4.0	>100
PD 824						
Methanol	0.2	190	10	3.5	0.2	>100
Ethanol	0.3	260	11	2.8	0.3	>100
Butanol	0.3	620	15	6	0.3	>100
Pentanol	0.3	860	8	1.8	0.4	>100
DMSO	0.4	890	16	35	0.4	>100
PC	0.4	990	16	1.5	0.5	>100

[a] τ_{10}, first excited-state lifetime; τ_r, orientational diffusion time; τ_{21}, higher-excited-state lifetime; τ_{gr}, ground-state recovery time; τ_{40}, decay time from the *cis* to the *trans*-states. Uncertainties: $\tau_{10}, \pm 10\%$; $\tau_r, \pm 15\%$; $\tau_{21}, \pm 15\%$; $\tau_{gr}, \pm 10\%$ to $\pm 20\%$; $\tau_{41}, \pm 30\%$ to $\pm 20\%$. Uncertainties in τ_{gr} and τ_{14} depend on the relative lifetimes between the two of them and their connection by Eq. (3).

[b] DNF, did not fit.

[c] NA, not applicable because parameters were not required.

take extra care with respect to the photostability of the molecules under high irradiance excitation. It was shown that the photochemical decomposition of the molecules can lead to an increase in the linear transmission during the data acquisition, thus reducing the nonlinear response at high inputs.[5] Figure 5 shows nonlinear transmission curves for PD 1952 in ethanol at repetition rates of 10 Hz (1), 5 Hz (2), and 1 Hz (3). Increasing the time between pulses led to a partial recovery of transmission values due to diffusion of fresh molecules into the focal volume, thus decreasing the photobleaching effect. It can be seen from Fig. 5 that the measurements at different repetition rates start to diverge at a fluence of ~ 0.1 J/cm^2 (~ 4.5 GW/cm^2). Below these values, the photodegradation is negligible. For future reference we define a turning point as the input at which the transmittance stops decreasing and starts increasing.

On the basis of the results of Fig. 5, all nonlinear transmission curves were taken at 10 Hz up to fluences of ~ 0.01 J/cm^2, and then the data were taken at 1 Hz with the sample moved (perpendicular to the input beam direction) between each shot, to make sure a fresh part of the sample is irradiated. The results for each dye in a different host solvent are shown in Fig. 6 along with the numerical fits using the four-level model; note that the first excited-state cross section (σ_{12}) is not a fitting parameter and is that determined from the Z scans. The nonlinear transmission data do not fit well at fluences above the

turning point for all dyes. This effect is more pronounced for the dicarbocyanine and tetracarbocyanine [Figs. 6(a) and 6(e)], since their turnover point is at a much lower fluence. Ground- and excited-state cross sections and their ratios and lifetimes determined from the experiments and modeling fits for all dyes in different solvents are summarized in Tables 3 and 4.

B. Nanosecond Results and Modeling

Similar to the goal for the picosecond measurements, the nanosecond experiments are performed to determine the molecular parameters that affect nonlinear absorption in the nanosecond regime and to investigate how the structure and solvent affect these parameters. The energy-level models developed from the picosecond regime are the starting point for developing models for the nanosecond regime that fit both the Z-scan and nonlinear transmission experiments. In this subsection we will describe the results of the experiments as well as the energy-level models.

The first nanosecond experiments carried out were low-energy Z scans, in which the same three-level model and molecular parameters are used to fit the results. As with the picosecond Z scans, the nanosecond measurements were performed at the peak of the ESA spectrum for each dye. Figure 7(a) shows a typical result for the Z-scan experiment with the fitting using the three-level all-singlet model. Figure 7(b) shows the excited-state cross section

Table 4. Nonlinear Absorption Properties

Dye (ESA Peak λ)	Peak GS Cross Section[a] ($\times 10^{-15}$ cm^2)	GS at ESA Peak Cross Section ($\times 10^{-18}$ cm^2)	α Peak Pico	α Peak Nano	GS at 532 nm Cross Section ($\times 10^{-18}$ cm^2)	α 532 nm	β
PD 2350 (500 nm)							
Methanol	0.88	5.4	46	46	24.5	2.8	2
Ethanol	0.90	4.7	45	55	29.0	2.5	2.2
Butanol	0.89	4.1	62	60	15.0	3.8	2.3
Pentanol	0.83	7.3	40	42	29.0	3.0	2.5
DMF	0.83	6.6	45	38	21.0	5.0	2.4
DMSO	0.91	4.2	66	58	18.2	5.0	2.6
MF	0.66	4.3	54	66	16.9	5.3	2.4
PC	0.84	6.7	43	50	25.3	3.5	2.3
PD 1952 (532 nm)							
Methanol	1.02	3.1	84	70	Peak at 532		7
Ethanol	1.12	2.2	128	95			6.8
DMF	0.90	4.5	55	55			4.5
DMSO	0.82	3.1	78	48			5.2
MF	0.70	1.9	122	162			5.2
PC	0.85	2.6	95	98			6.3
PD 2410 (594 nm)							
Methanol	0.92	119	3.2	4.2	36.1	4.3	2.9
Ethanol	0.94	115	2.9	4.5	34.7	4	2.9
DMSO	0.72	94	2.4	3.9	28.4	4	2.4
PC	0.76	99	3.0	6.5	30	4.8	2.8
PD 3428 (532 nm)							
Methanol	1.10	6.3	50	87	Peak at 532		6
Ethanol	1.11	6.4	44	73			5.3
Butanol	1.02	6.0	30	57			4.8
DMF	0.77	7.7	34	36			4.8
DMSO	0.89	5.1	63	NM[b]			5.5
MF	0.74	4.3	65	90			4.3
PC	0.91	5.2	58	85			3.6
PD 824 (570 nm)							
Methanol	0.88	16.4	23	39	15.8	17	3.5
Ethanol	0.85	10.2	38	63	13.7	20	4.3
Butanol	0.90	7.5	52	80	16.2	12	2.8
Pentanol	0.29	7.9	41	49	10.7	25	3.8
DMSO	0.49	22.9	16	26	28.0	7	2.6
PC	0.32	7.8	39	60	7.8	24	2.6

[a]Peak GS Cross Section—ground-state (GS) cross section at peak spectral position. GS at ESA Peak Cross Section—ground-state cross section at peak spectral position of ESA spectrum. α Peak Pico—ratio of excited-state to ground-state cross sections. α Peak Nano—ratio of excited-state to ground-state cross sections. GS at 532 nm Cross Section—ground-state cross section at 532 nm. α 532 nm—ratio of excited-state to ground-state cross sections at 532 nm. β—ratio of higher-excited-state cross section to ground-state cross section at 532 nm. Uncertainties: peak GS cross section, ±5%; GS at ESA peak cross section, ±8%; α, ±10%; β, ±20%.

[b]NM, not measured.

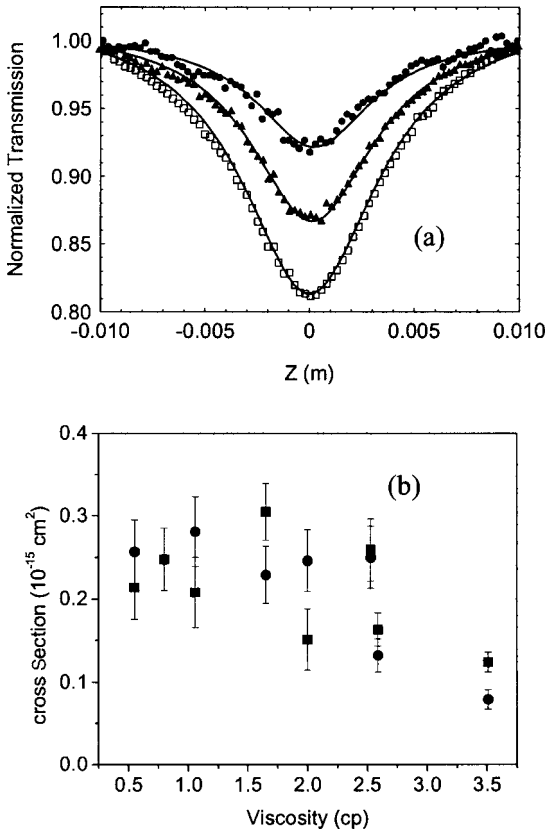

Fig. 7. (a) Nanosecond Z-scan results for PD 2410 in ethanol at fluences of 5.8×10^{-3} J/cm^2 (circles), 11.5×10^{-3} J/cm^2 (triangles), and 23×10^{-3} J/cm^2 (squares); fitting parameters of $\sigma_{10}=1.2\times10^{-16}$ cm^2, $\sigma_{12}=3.8\times10^{-16}$ cm^2, and $\tau_{10}=1.2$ ns. (b) Comparison of the excited-state cross sections determined by the picosecond (circles) and nanosecond (squares) Z scans using the three-level model for PD 1952 plotted as a function of solvent viscosity.

for PD 1952 in all eight host solvents determined from the picosecond (circles) and nanosecond (squares) Z-scan measurements. As can be seen, excited-state cross sections for both picosecond and nanosecond results in different solvents are similar. Therefore the same three-level model used for low-energy picosecond pulses is valid for low-energy nanosecond Z scans. The nanosecond results are summarized with the picosecond results in Table 4, which is discussed in Subsection 4.C.

The first issue to be addressed concerning the nanosecond nonlinear transmission measurements is whether the four-level model used in the picosecond regime is valid in the nanosecond regime. From the results of the nanosecond Z scans, it looks promising that the four-level model will adequately describe the nonlinear transmission results. However, as can be seen in Fig. 8(a), the four-level model (dashed curve) overestimates the nonlinear transmission for fluences above 0.1 J/cm^2 in the nanosecond regime. Four out of the five dyes displayed the same trend, which indicates that another process is occurring on nanosecond time scales. The fact that the four-level model overestimates the nanosecond nonlinear transmission results implies that molecules are decaying to a new state that is not accounted for by the current model. If so, this new process must have a slow formation rate (more than hundreds of picoseconds), since it does not affect the picosecond nonlinear transmission (Fig. 6). As discussed in Ref. 5, triplet-state formation can be ruled out as commonly known intersystem crossing times for PDs are about 2 orders of magnitude longer than τ_{10} (typically, hundreds of nanoseconds). This leads us to believe that we are seeing the polymethines undergo a photoisomerization process from the first excited *trans* state (S_1) to a *cis* state (labeled as C_1) as shown in Fig. 8(b). It has been shown by several groups of investigators that carbocyanines readily undergo this photoisomerization process.[27–29]

The rate equations that describe the dynamics of the six-level model shown in Fig. 8(b), along with the propagation equation, are given as

$$\frac{\partial N_0}{\partial t} = -\frac{\sigma_{01} I}{\hbar\omega} N_0 + \frac{N_1}{\tau_{\mathrm{gr}}} + \frac{N_5}{\tau_{40}},$$

$$\frac{\partial N_1}{\partial t} = \frac{\sigma_{01} I}{\hbar\omega} N_0 - \left(\frac{1}{\tau_{\mathrm{gr}}} + \frac{\sigma_{12} I}{\hbar\omega} + \frac{1}{\tau_{14}}\right) N_1 + \frac{N_2}{\tau_{21}},$$

$$\frac{\partial N_2}{\partial t} = \frac{\sigma_{12} I}{\hbar\omega} N_1 - \frac{N_2}{\tau_{21}},$$

$$\frac{\partial N_4}{\partial t} = \frac{N_1}{\tau_{14}} - \left(\frac{\sigma_{45} I}{\hbar\omega} + \frac{1}{\tau_{40}}\right) N_4 + \frac{N_5}{\tau_{54}},$$

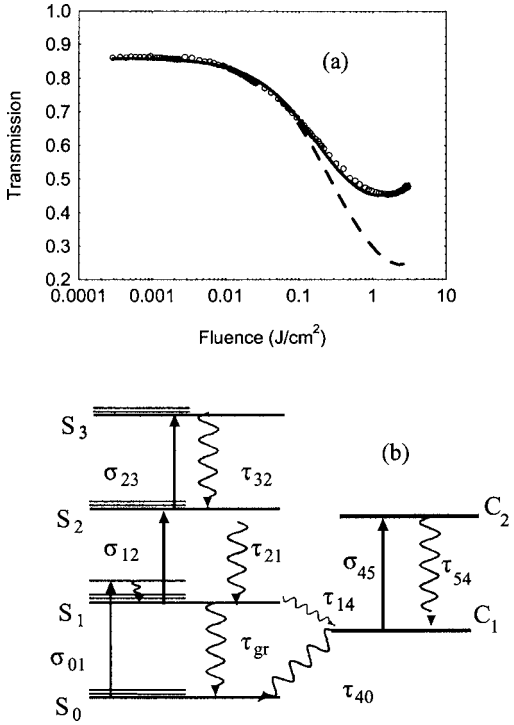

Fig. 8. (a) Nanosecond nonlinear transmission curves with fits for PD 824 in PC using the four-level model (dashed curve) and new six-level model (solid curve) shown in (b); (b) Six-level model to fit nanosecond nonlinear transmission curves composed of the four-level model with a new decay pathway from the first excited state to a *cis* state (C_1).

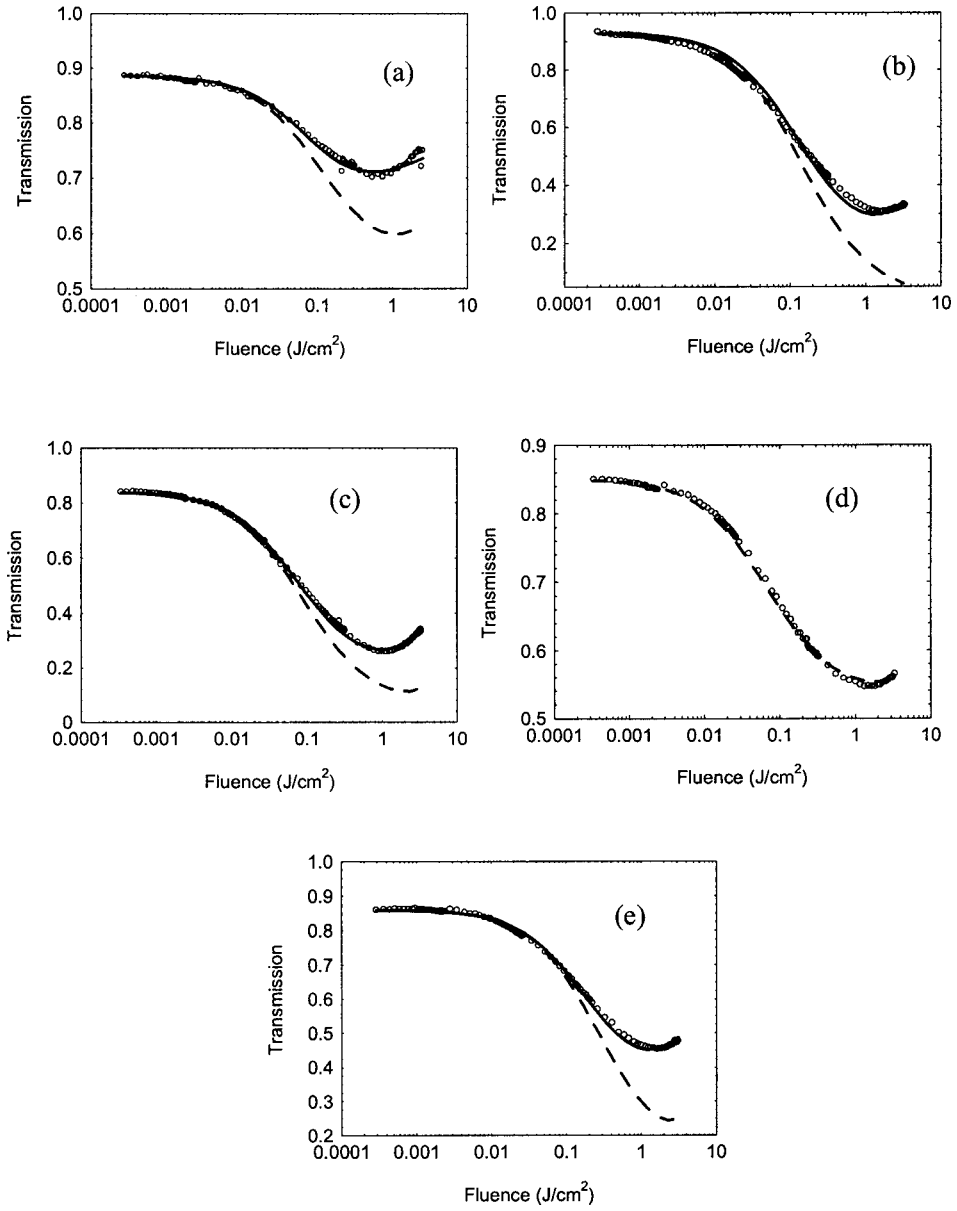

Fig. 9. Nanosecond nonlinear transmission curves with the 7 ns pulse width (FWHM) with fits using the four-level model (dashed curves) and six-level model without absorption from the *cis* state (solid curves) for (a) PD 2350 in DMF, (b) PD 1952 in ethanol, (c) PD 3428 in butanol, (d) PD 2410 in methanol, and (e) PD 824 in PC.

$$\frac{\partial N_5}{\partial t} = \frac{\sigma_{45} I}{\hbar \omega} N_4 - \frac{N_5}{\tau_{54}},$$

$$\frac{\partial I}{\partial z} = -I(\sigma_{01} N_0 + \sigma_{12} N_1 + \sigma_{23} N_2 + \sigma_{45} N_4), \tag{2}$$

where $N_{0,1,2}$ and $N_{4,5}$ are the respective level population densities of states $S_{0,1,2}$ and $C_{1,2}$ and are functions of time t and the propagation distance z; $N_0+N_1+N_2+N_3+N_4+N_5=N$, where N is the molecular density. $I(z,t)$ is the irradiance of the incident pulse, and $\sigma_{j(j+1)}$ and $\tau_{(j+1)_j}$ are the corresponding absorption cross sections and lifetimes, respectively. The effects of the vibronic sublevels are not accounted for in the rate equations owing to the fact that they have subpicosecond relaxation times; however, we are implicitly taking them into consideration so stimulated emission can be neglected. In addition, lifetime τ_{32} is assumed to be much less than the pulse width, resulting in negligible population of level three.

For the 7 ns pulsewidth, we initially neglect the absorption from the state C_1, so the only fitting parameters for this model are the formation (τ_{14}) and decay (τ_{40}) times of this new level. We show later that this assumption is valid. Up to this point, we have assumed only one excited-state decay pathway (directly to the ground state) with the rate measured by the picosecond pump–probe experiment. This is no longer the case, and the excited-state decay time (τ_{10}) must be divided between two pathways in the following manner [see Fig. 8(b)]:

$$\frac{1}{\tau_{10}} = \frac{1}{\tau_{14}} + \frac{1}{\tau_{\mathrm{gr}}}. \tag{3}$$

The nanosecond nonlinear transmission curves were measured with 7 ns FWHM pulses and, to try to have better access to this *cis* state, with 21 ns FWHM pulses. The results of both experiments are shown below. As with the picosecond nonlinear transmission measurements, all the nonlinear transmission curves were performed at 532 nm, the second harmonic of the Continuum Powerlite 9010.

Photodegradation in the nanosecond regime is not as big of an issue as in the picosecond regime owing to the lower irradiance. However, thermal nonlinearities are a concern in the nanosecond regime,[30] and care must be taken to avoid thermal defocusing, which can interfere with the experimental results in two ways. The most obvious way is that, owing to thermal lensing, the light is defocused so that it is not all collected by the detectors, thus artificially reducing the transmittance values. Even if extra lenses are added to guarantee that all light is collected, thermal defocusing can still affect the data analysis. The second effect is that, if the thermal nonlinearity is large enough, the beam size can change as it passes through the sample, so the thin-sample approximation is no longer valid.[31] Therefore, closed-aperture Z scans were performed at low and high energies for the two pulse widths used for the nonlinear transmission experiments. From these experiments we found that at the short pulse width the thermal nonlinearity was negligible, but, for the long pulse width, the thermal nonlinearity was substantial. To reduce the effect of the thermal nonlinearity at the long pulse width, we increased the spot size of the beam to 90 μm from 21 μm. For this spot size the thermal nonlinearity is negligible even for the longer pulse width. This is because the response time of the thermal nonlinearity is determined by the ratio of the spot size and the speed of sound in the medium, which for ethanol is 1000–1200 m/s.[31] For the small spot size the response time of the thermal nonlin-

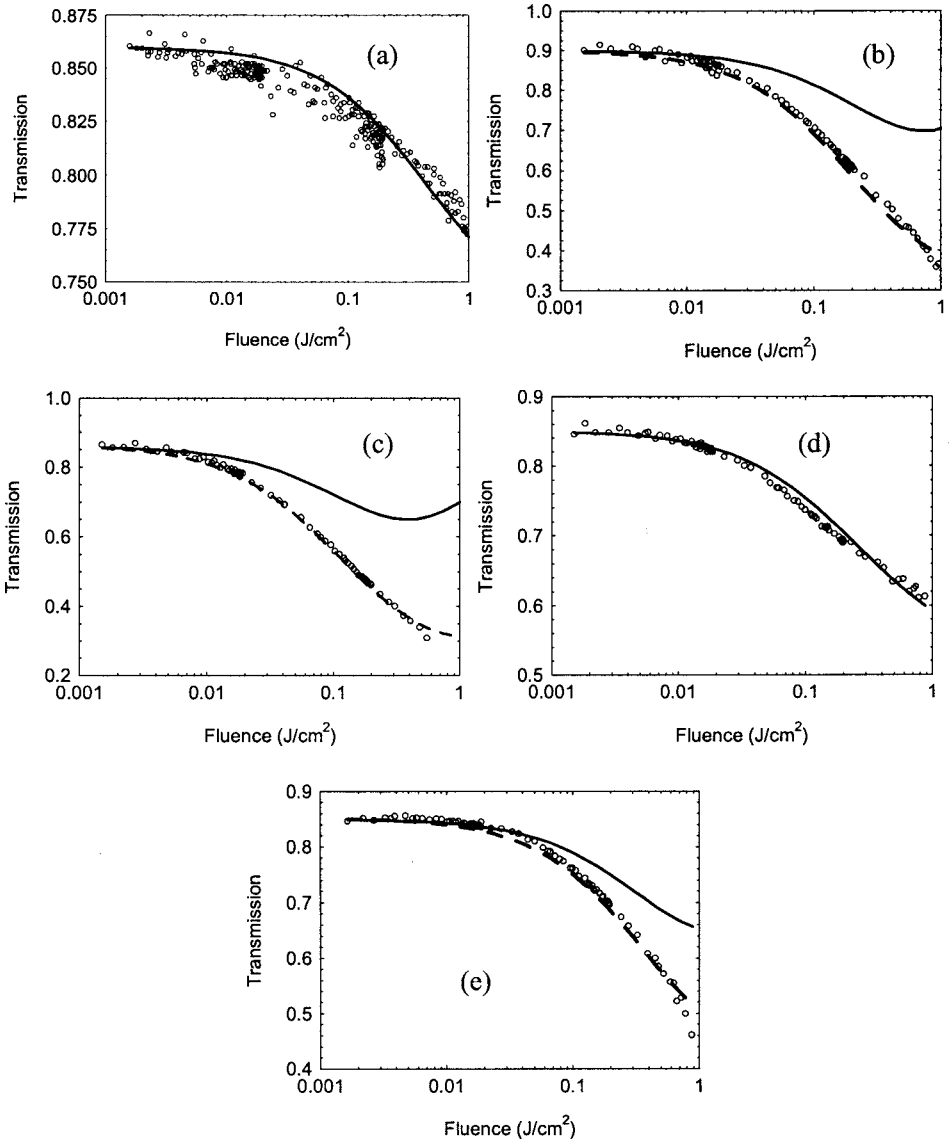

Fig. 10. Nanosecond nonlinear transmission curves using a 21 ns pulse width (FWHM) with fits using the six-level model without absorption from the *cis* state (solid curves) and the six-level-model with absorption out of the *cis* state (dashed curves) for (a) PD 2350, (b) PD 1952, (c) PD 3428, (d) PD 2410, and (e) PD 824 in ethanol. PDs 2350 and 2410 can be fitted with $\sigma_{45}=0$. For PD 1952 $\sigma_{45}=2.4\times10^{-17}$ cm^2, for PD 3428 $\sigma_{45}=5.0\times10^{-17}$ cm^2, and for PD 824 $\sigma_{45}=7.9\times10^{-17}$ cm^2.

earity can be calculated to be ~16 ns, and, for the large spot size, it is 75 ns.[32]

The nanosecond nonlinear transmission results using the 7 ns pulse width for each dye in different solvents are shown in Fig. 9 along with numerical fits using the four-level model (dashed curves) and the six-level model (solid curves). Even though photodegradation is not a major issue, the sample is still continuously moved transverse to the beam axis during the measurements. The fitting procedure for this data is, first, to determine the best-fit parameters using the four-level model and, second, to use these parameters as the starting point for the six-level model. The fits shown in Fig. 9 are some of the better fits, and, in general, the data could not be fitted as well as the picosecond nonlinear transmission curves. One possible explanation for this will be given below and discussed in more detail in Subsection 4.C. The lifetimes for the *cis*-state formation and decay are summarized in Table 3, along with the rest of the excited-state dynamic results, and will be discussed in Subsection 4.B.

The long-pulse-width (21 ns) nanosecond nonlinear transmission was performed for all dyes in ethanol only. The six-level model with the *cis*-state cross section (σ_{45}) as zero, which was used for the 7 ns data, fits only the experimental results for the dicarbocyanine dye [PD 2350, Fig. 10(a)] and the conjugated bridge tricarbocyanine dye [PD 2410, Fig. 10(d)]. For fitting the nonlinear transmission results for the other molecules, the absorption out of the *cis* state had to be included. Currently, the information about the nature of this *cis* state is not known completely. With the *cis*-state ESA cross section and the excited-state lifetime of this state unknown, the fits can only be approximated. The experimental data with fitting by the six-level model with σ_{45} as zero (solid curves) and the six-level model with *cis*-state absorption (dashed curves) are shown in Fig. 10. The characteristics of the *cis*-state absorption properties are discussed and shown in Subsection 4.C. The data for the decay of the excited-state *cis* state are discussed in Subsection 4.B. We also note here that the model for fitting the 21 ns data also fit the 7 ns and picosecond data. Hence, one set of parameters fits all of the data from 21 ns to 24 ps.

4. RESULTS AND DISCUSSION

A. Excited-State Absorption Spectra

The ESA spectra were initially performed only to determine the peak of the absorption for the nonlinear optical characterization measurements. However, by examining these spectra, one can uncover key insights into the nature of ESA as a function of conjugation length and bridge structure. The ESA spectra along with the corresponding linear absorption spectra for each of the six dyes in ethanol are shown in Fig. 11.

First, we will examine how the bridge structure affects the ESA spectrum by comparing the spectra of PD 3428 [unbridged, Fig. 11(c)], PD 1952 [dimethylene bridge, Fig. 11(b)], and PD 2410 [vinylene bridge, Fig. 11(d)]. The most obvious feature is that the bridged structures have only a single peak in the ESA spectrum, whereas the unbridged structure possesses a double peak. Another important feature is the large redshift in the peak of the ESA spectrum (to ~590 nm) of the conjugated bridge (PD 2410), whereas the unconjugated bridge (PD 1952) peak remains at the same wavelength (~532 nm) as the unsubstituted chromophore (PD 3428). It is interesting to note that, though the shape of the ESA spectra has been altered owing to the bridge structure, the peak ESA cross section of all three dyes are equal to within 20%.

Next we will examine the ESA spectra of the unsubstituted dicarbocyanine and tricarbocyanine dyes (PD 2350 and PD 3428) along with the substituted tetracarbocyanine and pentacarbocyanine dyes (PD 824 and PD 1659). The ideal case would be to examine an entire series of unsubstituted dyes from dicarbocyanine to pentacarbocyanine, but the tetracarbocyanine and pentacarbocyanine dyes are unstable in an unsubstituted form. The general characteristics of the linear absorption spectrum of polymethine molecules as the conjugation length is increased were discussed in Section 1. The main properties are a redshift and broadening (especially for PD 1659) of the linear absorption band as the conjugation length is increased. We are now in position to make a comparison between these linear absorption band properties and the ESA band properties.

First, we examine the redshift of the ESA spectrum as a function of conjugation length compared with that of the linear absorption spectrum. Figure 12(a) shows the absorption maximum for the linear (squares) as well as the ESA (circles) absorption profiles from dicarbocyanine to pentacarbocyanine. As can be seen, the linear absorption peak shifts by over 350 nm, while the ESA peak shifts by only 120 nm. This relatively small shift in the ESA spectrum as a function of conjugation length could have important consequences for the design of broadband nonlinear devices using polymethines. In certain cases this small shift could be advantageous because it allows the possibility of combining several dyes of different conjugation lengths that have their linear absorption peaks outside the visible range but have partially overlapping ESA spectra to adequately cover a large range of the visible spectrum.

The second interesting characteristic to compare is the spectral width of the ESA band and that of the linear absorption band. It is more meaningful to look at a frequency scale when one compares widths of spectra, since it is directly proportional to the energy. Figure 12(b) shows the FWHM in wavenumbers (inverse centimeters) of the linear (squares) and ESA (circles) absorption bands. From this picture it can be clearly seen that, whereas the linear absorption width stays nearly constant up to the tetracarbocyanine, the ESA spectral width continuously decreases. It is also instructive to compare the integrated area $[\int \alpha(\nu) d\nu]$ of the absorption bands, since it is directly related to the oscillator strength of the transition.[33] The integrated areas of the linear and ESA absorption bands are shown in Fig. 12(c). The main characteristic to note is that, as the conjugation length is increased, the areas of the linear and ESA absorption bands become similar. The ratio of these two areas is shown in Fig. 12(d). This is an important result because this shows that as the conjugation length is increased the oscillator strength of the excited state becomes larger in proportion to the ground-state oscillator strength. For example, for

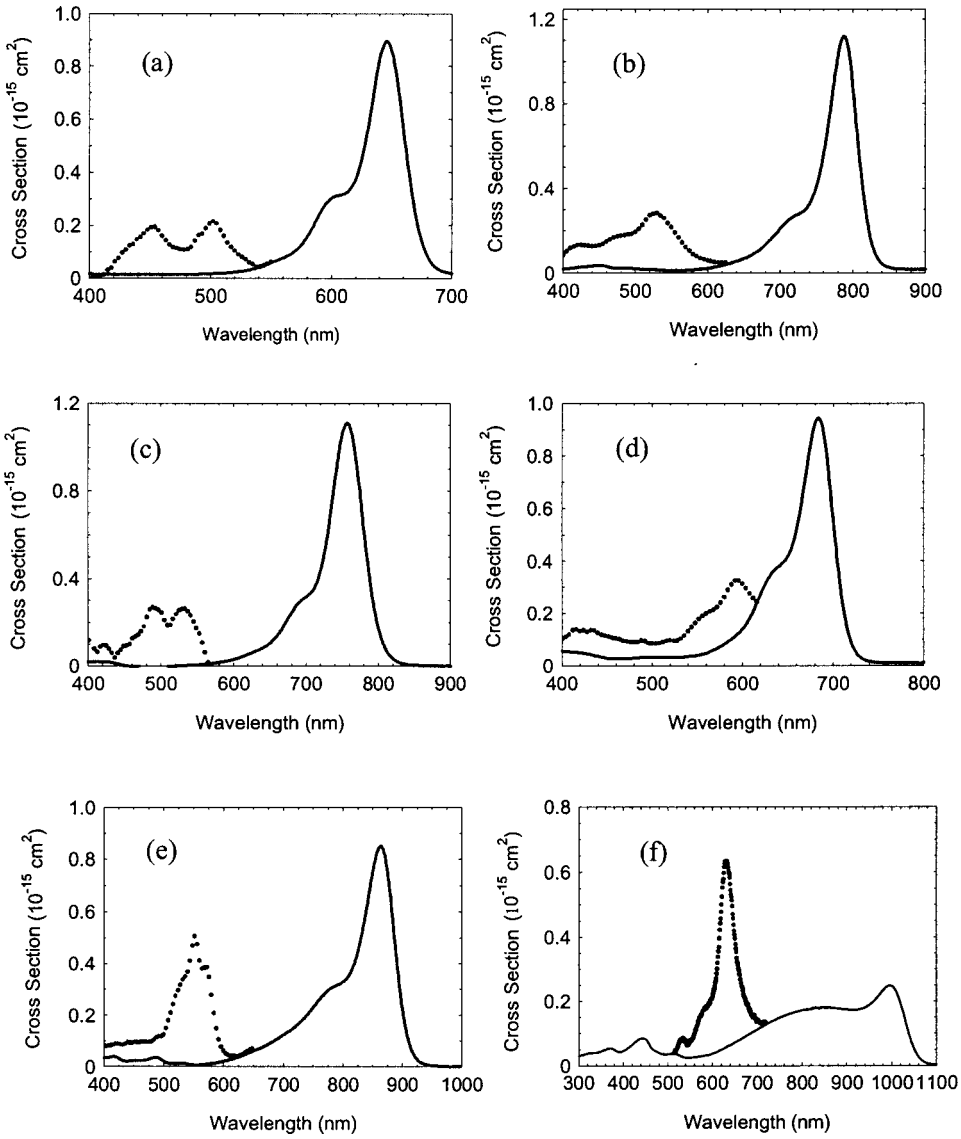

Fig. 11. ESA spectra for (a) PD 2350, (b) PD 1952, (c) PD 3428, (d) PD 2410, (e) PD 824, and (f) PD 1659 in ethanol. Solid curves are the linear absorption spectra, and dotted curves are the ESA spectra.

pentacarbocyanine dye, PD 1659, the excited-state oscillator strength is nearly 90% of the ground-state oscillator strength. This large oscillator strength means that the excited-state cross section can be as large as (or may be even larger than) the maximum ground-state cross section, as can be seen in Fig. 11(f).

The final characteristic we examine is the shape of the ESA spectrum from the dicarbocyanine to pentacarbocyanine molecules. It can be seen in Fig. 11(a) that for the dicarbocyanine molecule there are two clearly resolvable peaks in the ESA spectrum separated by 50 nm. As the conjugation length is increased to tricarbocyanine and tetracarbocyanine, the separation between these two peaks decreases to 40 and 20 nm, respectively. For the pentacarbocyanine shown in Fig. 11(f), the ESA spectrum has only a single peak. The reason for this decrease in separation between the two peaks is still being investigated but is probably connected with the formation in the S_1 state of two differently charged forms of polymethine molecule with symmetrical and asymmetrical charge distributions as described in Ref. 9. Each of these forms can take part in the ESA process, and an increase of the chain length leads to a more symmetrical charge distribution in S_1 reflected by the shape of the ESA band. However, a clearer picture requires additional experimental and theoretical studies.

B. Excited-State Dynamics

In this subsection the ESA dynamics of the polymethine molecules is discussed. This includes the dynamics directly measured by the pump–probe experiments (i.e., excited-state decay and orientational diffusion[11]) and those determined indirectly from the fitting of picosecond and nanosecond data (i.e., higher-excited-state decay, ground-state recovery, *cis*-state formation and decay). The decay of the *cis* excited state (τ_{54}) determined from the fitting of the six-level model was found to be of the order of 20 ps for PD 824 and of the order of 100 ps for both PD1952 and PD3428. This implies that the lifetime of the upper *cis* state is approximately an order of magnitude

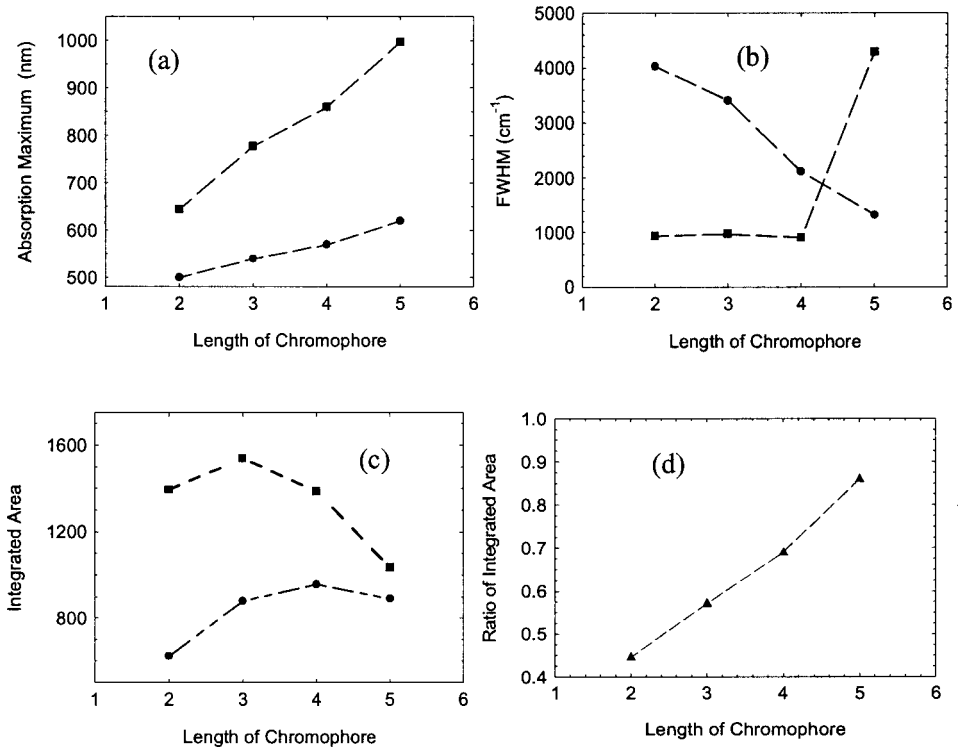

Fig. 12. Analysis of ESA spectra plotted as a function of conjugation length from dicarbocyanine to pentacarbocyanine dyes: (a) peak of linear (squares) and ESA (circles) spectra, (b) FWHM (inverse centimeters) of linear (squares) and ESA (circles) absorption bands, (c) integrated areas of linear (squares) and ESA (circles) absorption bands, and (d) ratio of integrated areas of ESA to linear absorption bands.

longer than the upper lifetime of the *trans* state. Also, the upper lifetime of the *cis* state appears to get longer with increasing conjugation length, whereas the upper lifetime became shorter with increasing conjugation length of the *trans* state. All other excited-state dynamic results are displayed in Table 3.

First, we examine the energy-level kinetics. In this analysis we are trying to identify the kinetics that are beneficial for picosecond and nanosecond nonlinear absorption and the connection of these model parameters to the molecular and solvent parameters. A long excited-state lifetime ($\tau_{10}>$ pulse width, in this case nanoseconds) has often been regarded as a key molecular parameter for efficient nonlinear absorption.[2,3] Therefore, understanding the connection between conjugation length and solvent properties on excited-state lifetime is important. Figure 13 shows the dependence of excited-state lifetime on conjugation length and demonstrates that for polymethines with chain lengths longer than tricarbocyanine the excited-state lifetime drops off dramatically. This does not mean that all polymethines with chain lengths longer than tricarbocyanine will be poor nonlinear absorbers; however, it does mean that the other molecular parameters will need to be able to compensate for this deficiency (i.e., large cross sections).

The excited-state decay pathway also plays a crucial role in the overall nonlinear performance. At high fluence levels in the nanosecond regime, in which the *cis* state can be populated, it is shown by Eq. (3) that the excited-state decay has two pathways. In cases in which the excited-state decay time (τ_{10}) is close to or equal to the

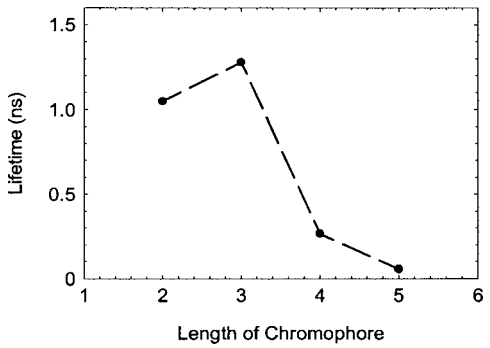

Fig. 13. Excited-state lifetime as a function of conjugation length for dicarbocyanine to pentacarbocyanine in ethanol.

ground-state recovery time (τ_{gr}), the four-level model applies. This case is shown in Fig. 9 (dashed curves), and better performance is observed. In contrast, where there is a large difference between τ_{10} and τ_{gr}, a large population in the weakly absorbing *cis* state is built up (short τ_{14}), thus hindering the performance. The dicarbocyanine (PD 2350) and conjugated bridge tricarbocyanine (PD 2410) dyes appear to be the most rigid molecules out of the five studied, having the longest formation time for the *cis* state. Two other tricarbocyanines (PD 1952 and PD 3428) have *cis*-formation rates of the same order as their excited-state lifetime. The dye with the long chain length, the tetracarbocyanine (PD 824), possesses a *cis*-formation rate an order of magnitude larger than its excited-state lifetime.

The effect of the higher-excited-state lifetime on picosecond nonlinear absorption has been discussed previously.[22] The fact that the higher excited state has a finite lifetime is the cause of the saturation effect in the picosecond regime. Molecules with shorter higher-excited-state lifetimes will be stronger picosecond nonlinear absorbers. This is due to the fact that the shorter the lifetime the faster the molecules return to the first excited state and can be reabsorbed by the same pulse. This lifetime, however, has no observable effect on the nanosecond absorption. Also, the recovery time from the *cis* state back to the *trans* state (τ_{40}) appears to be much longer than the pulse width, independent of the solvent. From the fitting, we can put only a lower limit on this time of ~100 ns.

C. Excited-State Orientational Diffusion

The final dynamic property we want to cover in this section is an analysis of the orientational diffusion times of the molecules. The Stokes–Einstein–Debye (SED) model describes rotational motion of the molecule as a hydrodynamic friction arising from the bulk viscosity of the solvent and neglects the molecular-level details of solute–solvent interactions. When dealing with solute molecules in polar solvents, one needs to consider the additional friction to rotational motion arising from electrostatic coupling, in the absence of specific interactions. The modified SED model, which includes the Perrin shape factor (f) and dielectric friction (τ_{DF}), is given as

$$\tau_r = \frac{\eta V}{KT} f C_{\text{bnd}} + \tau_{DF}, \tag{4}$$

where C_{bnd} is a constant that describes the boundary conditions, in which $C_{bnd}=1$ for the stick condition and $0 \leqslant C_{bnd} < 1$ for the slip boundary condition.[14,15,19] The simplest method for determining the slip condition was proposed by Hu and Zwanzig[34] and takes into account only the size and shape of the solute molecule. More recent theories have considered both the solute and solvent's sizes and shapes and the interaction between them.[15] In this paper we will consider only the Hu and Zwanzig slip boundary condition. The Perrin shape factor (f) corrects for the nonspherical shape of the polymethines by assuming the shape to be a prolate ellipsoid of revolution. f is given as

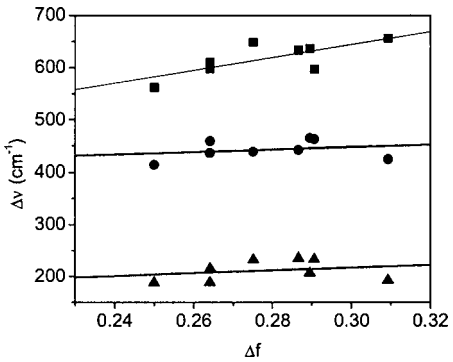

Fig. 14. $\Delta\nu$ versus polarity for PD 3428 (squares), PD 2350 (circles), and PD 1952 (triangles) with fits using the Lippert–Mataga equation. Fit parameter $a=6.4$ Å for PD 3428, $a=4.5$ Å for PD 1952, and $a=4.8$ Å for PD 2350.

$$f = \frac{2}{3} \frac{1-\rho^4}{(2-\rho^2)\dfrac{\rho^2}{\sqrt{1-\rho^2}} \ln\left(\dfrac{1+\sqrt{1-\rho^2}}{\rho}\right) - \rho^2} \quad \rho < 1, \tag{5}$$

where ρ is the ratio of the average of the lengths of the two short axes to that of the long axis of the ellipsoid.[19] The shape factor of the polymethines ranges from 1.94 for PD 2410 up to 3.4 for PD 3428.

The dielectric friction term is given as

$$\tau_{DF} = \frac{\mu^2}{9a^3kT} \frac{(n^2+2)^2\left[\epsilon(0)-n^2\right]}{\left[2\epsilon(0)+n^2\right]^2} \tau_D, \tag{6}$$

where μ is the excited-state dipole moment, a is the cavity radius that the solute molecule rotates within, and τ_D is the dielectric relaxation time of the solvent.[15] The cavity radius (a) is calculated in two different ways in the literature to give a maximum value and a minimum value.[19] The method to determine the minimum value of the cavity radius is to treat the Van der Waals volume of the solute molecule as a sphere and calculate the radius. The second method, which gives the maximum value, is to take half the length of the long axis of the molecule. From these two methods the minimum cavity radius of the polymethines is ≈4.8 Å, and the maximum value is ≈11 Å.

To calculate the dielectric friction contribution to the reorientational diffusion time, one must determine the excited-state dipole moment and correct cavity radius (between maximum and minimum values) of the molecules. The excited-state dipole moments are determined from quantum-chemical calculations and are presented in Table 1. To determine the correct cavity radius, we turn to the Lippert–Mataga equation, given by Eq. (1), and fit the difference between the absorption and the fluorescence peaks ($\Delta\nu$) as a function of polarity. We performed this analysis for the dicarbocyanine and tricarbocyanines. For tetracarbocyanine (PD 824) and pentacarbocyanine (PD 1659) molecules, the fluorescence measurement could not be performed owing to the infrared limit of the spectrofluorimeter. The results for PD 3428 (squares), PD 2350 (circles), and PD 1952 (triangles) are shown in Fig. 14. From this analysis we drew two important conclusions. First, the linear dependence of solvatochromic shifts on solvent polarity indicates the absence of a specific interaction or nonpolar solvatochromism, which is typical for cationic molecules with the charge symmetrically distributed within the polymethine chromophore.[9] Second, this data allow us to determine the correct cavity radii, which in all cases are closer to the minimum values.

Ultimately, we want to be able to examine the orientational diffusion time including the contributions of the dielectric friction as a function of viscosity for all the molecules studied. As can be seen in Eq. (6), the dielectric friction term is a function of the dielectric constant, index of refraction, and dielectric relaxation time. Therefore, to include the dielectric friction contribution, we had to develop a relationship between these parameters and the viscosity. For the alcohols, these three parameters relate to the viscosity monotonically, meaning it is possible to fit them with a polynomial and get an accurate relationship between them and their viscosity. The aprotic solvents do

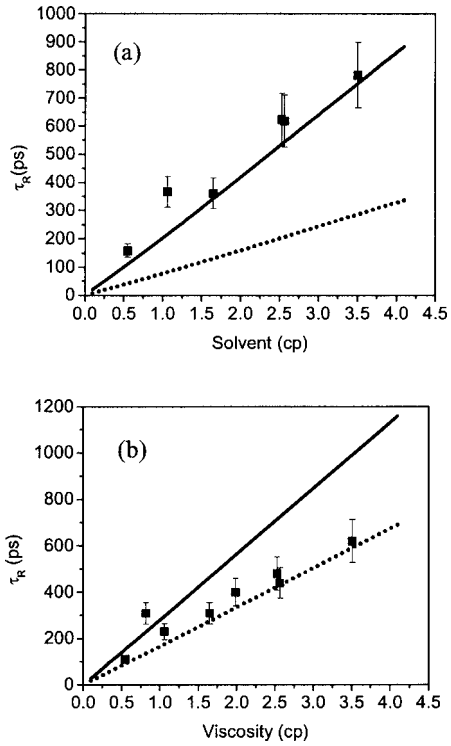

Fig. 15. Orientational diffusion times and fits with a stick boundary condition (solid curves) and slip boundary condition (dotted lines) for (a) PD 1952 and (b) PD 2350.

not have a monotonic trend. From the solvatochromic shifts (Fig. 14) we observed no difference between protic and aprotic solvents (nonpolar solvatochromism). This indicates that no error is introduced by not directly taking into account the aprotic nature of the solvents for the dielectric friction term.

The experimentally measured orientational diffusion times (the method is discussed in Refs. 10 and 11) and fits given by Eq. (4) with a stick boundary condition ($C_{\mathrm{bnd}}=1$), shown as solid curves, and a slip boundary condition based on tabulated data of Hu and Zwanzig,[34] shown as dotted lines, for PD 1952 ($C_{\mathrm{bnd}}=0.41$) and PD 2350 ($C_{\mathrm{bnd}}=0.53$) are presented in Fig. 15. The main characteristic to note is that PD 1952 follows the stick boundary condition, whereas PD 2350 follows the slip boundary condition, at least starting from the viscosity values of more than 1 cp. In fact, PD 2350 is the only dye among those investigated that follows a slip boundary condition. The reason for this is not obvious but could be connected with the fact that this molecule has the shortest length of polymethine chain studied, a planar-optimized geometry with small projections to the y and z axes, and flexible tails near the nitrogen atoms that can be packed into the relatively small cavity volume. This is in contrast to the phenyl rings in PD 3428 that are positioned perpendicular to the molecular plane, causing an additional friction to rotational motion.

D. Nonlinear Absorption Spectra

In this subsection we are concerned with identifying the effects of conjugation length, bridge structure, and host solvent on the overall ESA properties of the five polymethines and how these parameters apply to nonlinear absorption. This will include an analysis of how the molecular and solvent parameters affect the cross sections (ground, first, and higher excited states and *cis* state). Given this analysis, we will be in a good position to examine the nonlinear transmission curves spanning from the picosecond to the nanosecond time regimes. The absorption from the *cis* state can only be approximated owing to the fact that the inclusion of absorption from this state gives too many free parameters to model to make an accurate determination. These cross sections are $(2.4-7.9)\times10^{-17}$ cm^2 for the three molecules PD 3428, PD 1952, and PD 824 requiring absorption out of the *cis* state. The data for all other cross sections are displayed in Table 4. The results of the picosecond and nanosecond Z scans are displayed as "α Peak Pico" and "α Peak Nano," respectively, and are the ratios of the ESA cross sections to the ground-state cross section at the peak of the ESA. The column "α 532 nm" is the ratio used in the nonlinear transmission experiments and was determined from using the ESA spectra to extrapolate from the peak to 532 nm. The higher excited state is given as β and is also in reference to 532 nm. As can be seen in Table 4, the discrepancy between the results of the picosecond (α pico) and nanosecond (α nano) Z scans is larger than the experimental error for PD 3428 and PD 824. This could be due to absorption of the *cis* state, which seems to have the largest contribution for the unbridged tricarbocyanine (PD 3428) and the tetracarbocyanine (PD 824).

First, we examine the results of the linear absorption measurements and the Z scans, which provide information about the ground-state and first excited-state cross sections, respectively. Figure 16(a) shows the ground-state (squares) and excited-state (circles) cross sections for PD 1952 in all host solvents. As can be seen in the figure and from Table 4, there is no strong connection between the solvents and the peak ground-state cross sections, which have values of the order of 10^{-15} cm^2. The only noticeable trend is that the ground-state cross sections are, on average, 5%–15% smaller in the aprotic solvents. But, as can be seen from the excited-state cross sections [circles in Fig. 16(a)], this small variation in the peak ground-state cross sections has no noticeable connection to the ESA cross sections. It is also interesting to compare the peak ground-state cross sections to the cross sections at the wavelengths at which the nonlinear optical measurements are performed. For PD 2350, PD 1952, and PD 3428 the values of the ground-state cross sections at the wavelength of the peak ESA spectra are 2–3 orders of magnitude smaller. For these values of the ground-state cross sections, the concentrations of these three dyes in all nonlinear optical measurements are $\sim10^{-4}$ M ($T_L\approx0.80$). For PD 2410 and PD 824, the difference in cross sections is only 1 order of magnitude owing to the redshift of the ESA peak for PD 2410 and the broadening of the linear absorption spectrum for PD 824. This smaller difference is due to larger ground-state cross sections for the nonlinear measurements, and hence the concentration is smaller ($\sim10^{-5}$ M) for the same linear transmittance $T_L\approx0.80$. This makes the RSA easier to saturate in these materials. Photobleaching is also more likely in the less concentrated solutions and can also lead to the appear-

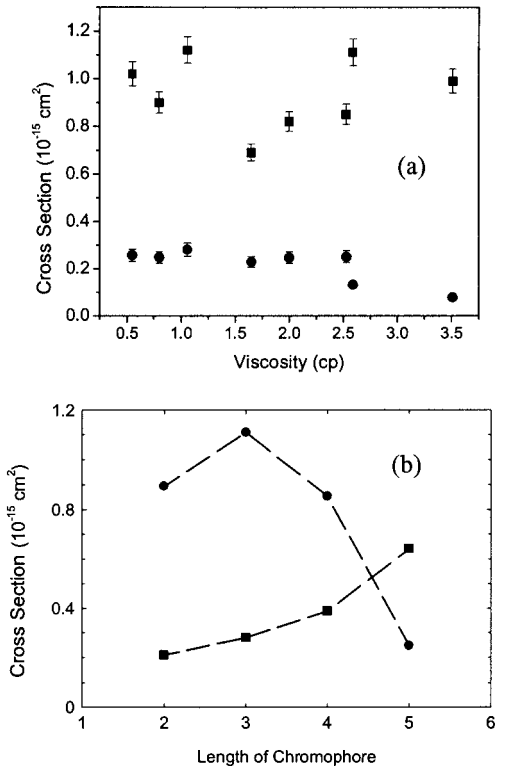

Fig. 16. Analysis of ground-state and ESA cross sections. (a) Ground-state (squares) and excited-state (circles) cross sections for PD 1952 in all host solvents plotted as a function of viscosity. (b) Peak ground-state cross section (squares) and excited-state cross section (circles) as a function of conjugation length (dicarbocyanine PD 2350, tricarbocyanine PD 3428, tetracarbocyanine PD 824, pentacarbocyanine PD 1659); all dyes in ethanol.

ance of saturation of the RSA. As can be seen in Fig. 6, the picosecond nonlinear transmission results show that PD 2350 and PD 824 saturate more quickly than is predicted by the four-level model, but this is not the case for PD 2410. This could be explained by the fact that PD 2410 has the smallest ratio of ground-state to excited-state cross sections ($\alpha=4$), so it is not easily saturated, whereas PD 824 and PD 2350 have large ESA and ground-state cross sections at 532 nm, resulting in fast saturation.

The peak ground-state and ESA cross sections as a function of conjugation length are shown in Fig. 16(b) and show that, though the peak of the ground-state cross section decreases as the conjugation length increases to tetracarbocyanine and pentacarbocyanine, the ESA cross section continuously increases until it becomes larger than the ground-state cross section. The ratio of integrated areas of the ground- and excited-state spectra was shown in Fig. 12(d). The usefulness of the pentacarbocyanine molecule for strong nanosecond nonlinear transmission is in doubt, owing to its poor photochemical stability and short excited-state lifetime ($\tau_{10}\approx 50$ ps).

The picosecond nonlinear absorption results not only provide information about the higher-excited-state cross sections of the polymethines but also, more importantly, allow us to determine characteristics of the polymethines that are ideal for large picosecond nonlinear absorption. The experimental data for all five dyes in one solvent and at a wavelength of 532 nm are shown in Fig. 17(a). In Fig. 17(a) the strongest nonlinear absorption in the picosecond regime is clearly seen for the tricarbocyanine dye, PD 1952, and the worst is for the dicarbocyanine dye, PD 2350. But performing an analysis in this way is rather misleading, since we are not at the peak of the ESA spectral position for each dye.

To make a direct comparison of the nonlinear absorption ability of each molecule, we must examine the nonlinear transmission at the peak of the ESA spectrum, remembering that all curves were taken at 532 nm. It is possible to get a good idea of what the overall nonlinear absorption performance would be at the peak of the ESA spectrum for each dye, since we have a reliable model for the picosecond regime, at least to the turning point, and knowledge of all molecular parameters (Tables 3 and 4). The only assumption we have to make in doing this is that the higher-excited-state cross section is a constant over this band, and, since we know this cross section at 532 nm, we can extrapolate what β would be at the peak of the ESA spectrum. This is a fair extrapolation because β really represents the conglomeration of all higher-excited-state absorption processes and will be relatively wavelength independent. Figure 17(b) shows the theoretical modeling of the picosecond curves for the five dyes at the peaks of their ESA spectra in methanol using the parameters from Tables 3 and 4.

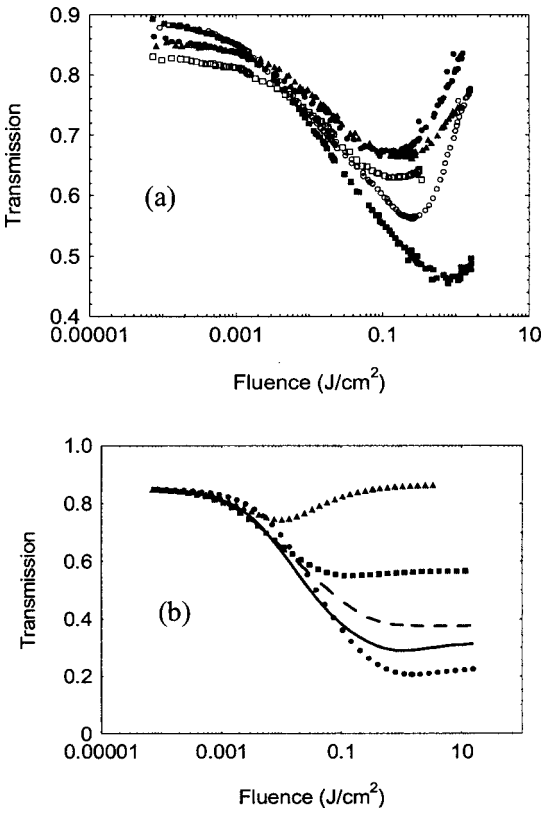

Fig. 17. (a) Experimental picosecond nonlinear transmission results for PD 2350 (triangles), PD 1952 (filled squares), PD 2410 (open squares), PD 3428 (open circles), and PD 824 (filled circles) in DMSO. (b) Picosecond nonlinear transmission using peak parameters for the five dyes in ethanol—PD 2350 (circles): $\alpha_{500}=46, \beta_{500}=9$; PD 1952 (solid curve): $\alpha_{532}=84, \beta_{532}=7$; PD 2410 (triangles): $\alpha_{594}=3.2, \beta_{594}=0.9$; PD 3428 (dashed curve): $\alpha_{532}=50, \beta_{532}=6$; PD 824 (squares): $\alpha_{570}=23, \beta_{570}=3.5$.

Since there is not a strong solvent dependence on the picosecond results, we will concentrate on examining the picosecond nonlinear transmission performance as a function of conjugation length and bridge structure by using the theoretical curves shown in Fig. 17(b). From looking at the experimental data in Fig. 17(a), one can see that one of the least effective RSA dyes at 532 nm is PD 2350; however, calculations show that it turns out to be the best at its peak ESA spectral position (500 nm). It not only has the largest change in transmission (75%) but also the highest turnover fluence (1.2 J/cm^2). This can be attributed to the fact that this molecule has the shortest higher-excited-state lifetime ($\tau_{21} \approx 2$ ps) and, on average, the second-largest ratio of excited-state to ground-state cross sections (α). PD 2410, which performed the third best in the experiments at 532 nm, would be the worst if the experiment is performed at its ESA spectral peak of 594 nm. This result is mainly connected with the large ground-state cross section (1.1×10^{-16} cm^2) at an ESA peak, which is nearly 2 orders of magnitude larger than for the other molecules. This results in the smallest α, of only 4. As can be seen in Fig. 17(b), this molecule saturates at an extremely low fluence level (0.01 J/cm^2) and has a change of transmission of only 13%, from which we can conclude that the conjugated bridge structure is detrimental to the ESA properties of polymethines—at least for picosecond nonlinear transmission. In order, from best to worst, the three remaining dyes rank as PD 1952, PD 3428, and PD 824. It is a little surprising that the tetracarbocyanine (PD 824), which has the largest excited-state cross section, performs worse than the two tricarbocyanines (PD 1952 and PD 3428). However, it has the smallest α and β, which results in a low saturation fluence of 0.13 J/cm^2. The short lifetime of PD 824 is not a contributing factor because even with a lifetime of the order of 200 ps it is still over an order of magnitude larger than the pulse width. PD 1952 and PD 3428 are quite similar in both maximum change of transmission ($\approx$60%) and turnover fluence ($\approx$0.75 J/cm^2), demonstrating that the unconjugated bridge has little effect on the ESA properties of the molecule.

Now we are in position to analyze the nanosecond nonlinear transmission results, since we have examined the picosecond nonlinear transmission results and have determined which molecules work the best. The results for all five dyes in one host solvent are given in Fig. 18(a). As can be seen in Fig. 18(a), the tricarbocyanines PD 1952 and PD 3428 are the two strongest nonlinear absorbers at 532 nm in the nanosecond regime, and the worst is the dicarbocyanine dye, PD 2350.

As with the picosecond measurements, to make a direct comparison of the overall nonlinear absorption ability of each molecule, we must examine the loss at the peak of the ESA spectrum. The theoretical curves using the six-level model are shown in Fig. 18(b) with the peak ESA spectral parameters given in Table 4 and β determined as discussed above. The dicarbocyanine dye, PD 2350, again has the best overall performance with the largest change in transmission ($\approx$95%) and the highest turnover fluence (13.4 J/cm^2). This dye has one feature, which is particularly attractive for nanosecond nonlinear absorption. As can be seen in Table 3, the ground-state recovery time is

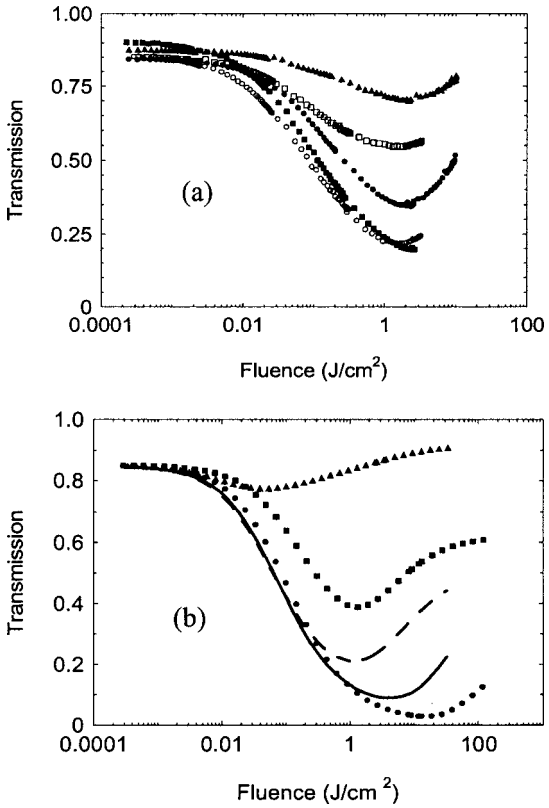

Fig. 18. (a) Experimental nanosecond nonlinear transmission results for PD 2350 (triangles), PD 1952 (closed squares), PD 2410 (open squares), PD 3428 (open circles), and PD 824 (closed circles) in ethanol. (b) Nanosecond nonlinear transmission using peak parameters for the five dyes in methanol—PD 2350 (circles): $\alpha_{500}=46, \beta_{500}=9$; PD 1952 (solid curve): $\alpha_{532}=84, \beta_{532}=7$; PD 2410 (triangles): $\alpha_{594}=3.2, \beta_{594}=0.9$; PD 3428 (dashed curve): $\alpha_{532}=50, \beta_{532}=6$; PD 824 (squares): $\alpha_{570}=23, \beta_{570}=3.5$.

close to the excited-state decay time, and the *cis*-transformation time is long (30 ns). This means that the molecule does not easily transform into the *cis* state. To fit the nanosecond nonlinear transmission data for PD 2410 in methanol and ethanol, one could use the four-level model without the addition of the *cis* state. However, owing to the reasons discussed in the picosecond analysis, this dye performs poorly in the nanosecond regime. Therefore, we can conclude that the conjugated bridge structure is good at stabilizing the *trans* state in some host solvents, but this advantage is far outweighed by the reduction in excited-state absorption properties compared with the unconjugated or unbridged structures, such as PD 1952 and PD 3428. These two tricarbocyanines, PD 1952 and PD 3428, as in the picosecond experiments, behave similarly in the nanosecond regime. The turnover fluence and change in transmission of PD 1952 and PD 3428 are 3.9 and 1.1 J/cm^2 and 90% and 75%, respectively. It is interesting to note that the gap in performance between the two tricarbocyanines and the dicarbocyanine has increased in the nanosecond regime. Whereas in the picosecond regime the turnover fluence for PD 2350 was twice as high as for the tricarbocyanines, it is, respectively, four and ten times larger for PD 1952 and PD 3428 in the nanosecond regime. This can be attributed to the fact that the tricarbocyanines are more easily converted

in to the *cis* state, thus reducing the population of molecules in the *trans* form. Interestingly, the nanosecond nonlinear absorption properties of the tetracarbocyanine PD 824 have been improved with respect to the other molecules. The turnover fluence for this molecule has improved by an order of magnitude to 1.4 J/cm^2, and its change in transmittance has also improved slightly to 54% from 36%. This could be due to the lower irradiance values in the nanosecond regime, so that photodegradation is not as much of a factor as it was in the picosecond regime. Also, as can be seen in Fig. 18(b), the onset of nonlinear absorption is at a higher fluence value than for the other molecules. This is due to the short excited-state lifetime of PD 824, which is approximately five times shorter than for the other molecules.

5. CONCLUSION

We have performed a detailed experimental investigation of five polymethines with chain lengths from dicarbocyanine to pentacarbocyanine in a large class of solvents to determine key molecular parameters for strong nonlinear absorption. By looking at the experimentally measured nonlinear transmission curves with a frequency-doubled Nd:YAG laser (532 nm wavelength), we found that the tricarbocyanines PD 1952 and PD 3428, which have an ESA peak near 532 nm, seemed to have the largest nonlinear loss and thus perform the best. But when theoretical curves were generated using molecular parameters at the peak of the ESA spectrum for each molecule, the result was different. The main result is that the shortest molecule studied (PD 2350) performed the best in both the picosecond and the nanosecond time regimes. The unconjugated bridge (PD 1952) and unbridged (PD 3428) molecules performed adequately, whereas the conjugated bridge molecule (PD 2410) performed poorly. The fact that the conjugated bridge structure reduces the effectiveness of the ESA properties is a little disappointing, since this type of bridge structure seemed to help stabilize the molecule in the *trans* state. The tetracarbocyanine PD 824 did not perform as well as the two tricarbocyanines but showed enough promise, so the other molecules of this chain length should be investigated. The main limitation of molecules of this or longer chain length appears to be photochemical stability.

In this study we investigated the ESA spectra of the five molecules in up to eight host solvents. From these spectra we not only determined at which wavelength to conduct the Z scans to measure the peak excited-state cross section but we also gained some insight into the nature of ESA in the polymethines. The main characteristic is that a larger percentage of the oscillator strength remains in the excited-state transition as the chain length is increased. This helps to explain the important result of measuring an excited-state cross section that is larger (about three times) than the ground-state cross section at the peak spectral position. We also observed that the shape of the ESA spectrum and the position of the ESA peak did not depend on the solvent. This simplified the nonlinear measurements, since each molecule in all solvents could perform at a single wavelength.

The analysis of the excited-state dynamics showed that the excited-state lifetime of molecules slightly increases as a function of the index of refraction of the solvent. The lifetimes of the dicarbocyanine and tricarbocyanines were of the order of 1 ns, whereas the tetracarbocyanine dye was only about 200 ps. The short lifetime of the tetracarbocyanine dye increased the fluence for the onset of nonlinear absorption by nearly an order of magnitude over the dicarbocyanine and tricarbocyanines. An analysis of the orientational diffusion times was also performed and shown that no specific solvent effects affected the rotational times of the polymethines. This could also be seen by examining the wavelength shift between the absorption and the fluorescence spectra as a function of the solvent. The orientational diffusion times could be predicted using the modified SED model including both the Perrin shape factor and the dielectric friction term. It was also found that four of the five polymethines studied in this paper followed a stick boundary condition, which makes sense, since the polymethine molecules are much larger than the solvent molecules. The shortest dye studied, PD 2350, followed a slip boundary condition, and the reasons for this are that this molecule has the shortest length of

Table 5. Molecular Parameters Determined from Experiments and Fits

Molecular Parameter	Experiment	Model Used to Fit Data
σ_{01}	Concentration-dependent linear absorption spectra	NA
σ_{12}	ps and ns Z scans	Three-level model
σ_{23}	ps nonlinear transmission	Four-level model
σ_{45}	21 ns nonlinear transmission	Six-level model with absorption from *cis* state
τ_{10}	ps pump–probe method	Equations from Refs. 10 and 11
τ_r	Ps pump–probe method	Equations from Refs. 10 and 11
τ_{21}	ps nonlinear transmission	Four-level model
τ_{32}	Always assumed instantaneous	NA
τ_{gr}	7 ns nonlinear transmission	Six-level model without absorption from *cis* state and Eq. (3)
τ_{14}	7 ns nonlinear transmission	Six-level model without absorption from *cis* state and Eq. (3)
τ_{40}	7 ns nonlinear transmission	Six-level model without absorption from *cis* state
τ_{54}	21 ns nonlinear transmission	Six-level model with absorption from *cis* state

polymethine chain, planar-optimized geometry, and flexible tails near the nitrogen atoms.

Picosecond and nanosecond Z scans were performed at the peak of the ESA spectrum for each molecule in all host solvents. For PDs 2350, 2410, and 1952 there is good agreement between the predicted excited-state cross sections from the picosecond and nanosecond results. For PDs 3428 and 824 the agreement was not as good as for the other dyes. This behavior may be explained by additional absorption from the *cis* state.

The picosecond and nanosecond nonlinear transmission results provided insight into the ESA properties of the polymethine molecule at high fluence levels. From this data we were able to develop energy-level models that can predict the nonlinear loss in polymethines from the picosecond to the nanosecond time regimes. Currently, the existence of a *cis* state can only indirectly be inferred from failure of the energy-level models developed from the picosecond data to accurately predict the nanosecond results at high fluences. The evidence, however, is quite strong that this is indeed the correct model to use. One example is that the short nanosecond pulse-width measurements for PD 2410 predicted that no *cis* state was present, and the long nanosecond pulse-width measurements agreed with this prediction. Also, the unbridged tricarbocyanine PD 3428, which should be the easiest to transform to a *cis* state, had the largest discrepancy between the four-level model and the nanosecond results. Finally, molecular parameters determined from experiments and model fits are summarized in Table 5. This table is meant to convey the fact that each fitting parameter is associated with an experiment. Therefore, for example, for the 21 ns data alone, a number of possible combinations of parameters could fit those data, but the parameters used, except for the *trans–cis* relaxation time, τ_{54}, were already determined from other experiments. Thus, the end result, Tables 3 and 4, shows the resulting experimentally determined values with the uncertainties noted.

ACKNOWLEDGMENTS

We gratefully acknowledge the support of the National Science Foundation ECS 0217932, the U.S. Army Research Laboratory, and the Naval Air Warfare Center Joint Service Agile Program (contract N00421-04-20001). Corresponding author J. Fu can be reached by e-mail at jfu@mail.ucf.edu. Corresponding author D. J. Hagan can be reached by phone, 407-823-6865; fax, 407-823-6817; or by e-mail, hagan@creol.ucf.edu.

*Current address, Optical Sciences Division, U.S. Naval Research Laboratory, Washington D.C., 20375-5338.

REFERENCES

1. J. W. Perry, "Organic and metal-containing reverse saturable absorbers for optical limiters," in *Nonlinear Optics of Organic Molecules and Polymers*, H. S. Nalwa and S. Miyata, eds. (CRC Press, 1997), pp. 813–840.
2. E. W. Van Stryland, D. J. Hagan, T. Xia, and A. A. Said, "Application of nonlinear optics to passive optical limiting," in *Nonlinear Optics of Organic Molecules and Polymers*, H. S. Nalwa and S. Miyata, eds. (CRC Press, 1997), pp. 841–860.
3. L. W. Tutt and T. F. Boggess, "A review of optical limiting mechanisms and devices using organics, fullerenes, semiconductors and other materials," Prog. Quantum Electron. **17**, 299–338 (1993).
4. O. V. Przhonska, J. H. Lim, D. J. Hagan, E. W. Van Stryland, M. V. Bondar, and Y. L. Slominsky, "Nonlinear light absorption of polymethine dyes in liquid and solid media," J. Opt. Soc. Am. B **15**, 802–809 (1998).
5. J. H. Lim, O. V. Przhonska, S. Khodja, S. Yang, T. S. Ross, D. J. Hagan, E. W. Van Stryland, M. V. Bondar, and Yu. L. Slominsky, "Polymethine and squarylium molecules with large excited-state absorption," Chem. Phys. **245**, 79–97 (1999).
6. D. A. Oulianov, A. S. Dvornikov, and P. M. Rentzepis, "Optical limiting and picosecond relaxation of carbocyanines upper electronic states," Opt. Commun. **205**, 427–436 (2002).
7. R. A. Negres, O. V. Przhonska, D. J. Hagan, E. W. Van Stryland, M. V. Bondar, Yu. L. Slominsky, and A. D. Kachkovski, "The nature of excited-state absorption in polymethine and squarylium molecules," IEEE J. Sel. Top. Quantum Electron. **7**, 849–863 (2001).
8. R. S. Lepkowicz, O. V. Przhonska, C. M. Cirloganu, D. J. Hagan, E. W. Van Stryland, M. V. Bondar, Yu. L. Slominsky, A. D. Kachkovski, and E. I. Mayboroda, "Absorption anisotropy studies of polymethine dyes," Chem. Phys. **306**, 171–183 (2004).
9. R. S. Lepkowicz, O. V. Przhonska, J. M. Hales, J. Fu, D. J. Hagan, E. W. Van Stryland, M. V. Bondar, Yu. L. Slominsky, and A. D. Kachkovski, "Nature of the electron transitions in thiacarbocyanines with a long polymethine chain," Chem. Phys. **305**, 259–270 (2004).
10. O. V. Przhonska, D. J. Hagan, E. Novikov, R. Lepkowicz, E. W. Van Stryland, M. V. Bondar, Yu. L. Slominsky, and A. D. Kachkovski, "Picosecond absorption anisotropy of polymethine and squarylium dyes in liquid and polymeric media," Chem. Phys. **273**, 235–248 (2001).
11. R. S. Lepkowicz, O. V. Przhonska, J. M. Hales, D. J. Hagan, E. W. Van Stryland, M. V. Bondar, Yu. L. Slominsky, and A. D. Kachkovski, "Excited-state absorption dynamics in polymethine dyes detected by polarization-resolved pump–probe measurements," Chem. Phys. **286**, 277–291 (2003).
12. G. R. Fleming, *Chemical Applications of Ultrafast Spectroscopy* (Oxford U. Press, 1986).
13. F. Perrin, "Mouvement brownien d'un ellipsoide (I). Dispersion dielectrique pour des molecules ellipsoidales," J. Phys. Radium **5**, 497–511 (1934).
14. M. Maroncelli, "Continuum estimates of rotational dielectric friction and polar solvation," J. Chem. Phys. **106**, 1545–1555 (1997).
15. G. B. Dutt, S. Doraiswamy, N. Periasamy, and B. Venkataraman, "Rotational reorientation dynamics of polar dye molecular probes by picosecond laser spectroscopic technique," J. Chem. Phys. **93**, 8498–8513 (1990).
16. M. Sheik-Bahae, A. A. Said, T. H. Wei, D. J. Hagan, and E. W. Van Stryland, "Sensitive measurement of optical nonlinearities using a single beam," IEEE J. Quantum Electron. **26**, 760–769 (1990).
17. M. Hamer, *The Cyanine Dyes and Related Compounds* (Interscience, 1964).
18. A. I. Tolmachev, Yu. L. Slominsky, and A. A. Ischenko, "New cyanine dyes absorbing in the NIR region," in *Near-Infrared Dyes for High Technology Applications*, S. Daehne, U. Resh-Genger, and O. S. Wolfbeis, eds., Vol. 52 of NATO Advanced Study Institute Series (Kluger Academic, 1998), pp. 385–415.
19. J. R. Lakowicz, *Principles of Fluorescence Spectroscopy*, 2nd ed. (Kluwer Academic/Plenum, 1999).
20. R. L. Fork, C. V. Shank, C. Hirlimann, R. Yen, and W. J. Tomlinson, "Femtosecond white-light continuum pulses," Opt. Lett. **8**, 1–4 (1983).
21. S. N. R. Swatton, K. R. Welford, S. J. Till, and J. R.

Sambles, "Nonlinear absorption of a carbocyanine dye 1,1',3,3,3',3'-hexamethylindotricarbocyanine iodide using a *z*-scan technique," Appl. Phys. Lett. **66**, 1868–1870 (1995).
22. R. S. Lepkowicz, A. Kobyakov, D. J. Hagan, and E. W. Van Stryland, "Picosecond optical limiting in reverse saturable absorbers: a theoretical and experimental study," J. Opt. Soc. Am. B **19**, 94–101 (2002).
23. S. Hughes and B. Wherrett, "Multilevel rate-equation analysis to explain the recent observations of limitations to optical limiting dyes," Phys. Rev. A **54**, 3546–3552 (1996).
24. X. Deng, X. Zhang, Y. Wang, Y. Song, S. Liu, and C. Li, "Intensity threshold in the conversion from reverse saturable absorption to saturable absorption and its application in optical limiting," Opt. Commun. **168**, 207–212 (1999).
25. A. Kobyakov, D. J. Hagan, and E. W. Van Stryland, "Analytical approach to dynamics of reverse saturable absorbers," J. Opt. Soc. Am. B **17**, 1884–1893 (2000).
26. T. Xia, D. J. Hagan, A. Dogariu, A. Said, and E. W. Van Stryland, "Optimization of optical limiting devices based on excited-state absorption," Appl. Opt. **36**, 4110–4122 (1997).
27. A. Sanchez-Galvez, P. Hunt, M. A. Robb, M. Olivucci, T. Vreven, and H. B. Schlegel, "Ultrafast radiationless deactivation of organic dyes: evidence for a two-state two-mode pathway in polymethine cyanines," J. Am. Chem. Soc. **122**, 2911–2924 (2000).
28. M. Levitus, R. M. Negri, and P. F. Aramdenia, "Rotational relaxation of carbocyanines. Comparative study with the isomerization dynamics," J. Phys. Chem. **99**, 14231–14239 (1995).
29. F. Momicchioli, I. Baraldi, and G. Berthier, "Theoretical study of *trans–cis* photoisomerism in polymethine cyanines," Chem. Phys. **123**, 103–112 (1988).
30. P. Brochard, V. Grolier-Mazza, and R. Cabanel, "Thermal nonlinear refraction in dye solutions: a study of the transient regime," J. Opt. Soc. Am. B **14**, 405–411 (1997).
31. J. Robertson, P. Milsom, J. Duignan, and G. Bourhill, "Spatial redistribution of energy in a nanosecond laser pulse by an organic optical limiter," Opt. Lett. **25**, 1258–1260 (2000).
32. D. I. Kovsh, D. J. Hagan, and E. W. Van Stryland, "Numerical modeling of thermal refraction in liquids in the transient regime," Opt. Express **4**, 315–327 (1999).
33. B. Valuer, *Molecular Fluorescence: Principles and Applications* (Wiley-VCH, 2002).
34. C. Hu and R. Zwanzig, "Rotational friction coefficients for spheroids with the slipping boundary condition," J. Chem. Phys. **60**, 4354–4357 (1974).